

A QCD BASED MODEL OF HADRON HADRON SCATTERING

Thesis by

Michael Phillip Shatz

In Partial Fulfillment of the Requirements

for the Degree of

Doctor of Philosophy

California Institute of Technology

Pasadena, California

1984

(Submitted May 22, 1984)

## ABSTRACT

The leading log approximation to Quantum Chromodynamics is derived, including the effects of gluon spin. The use of the leading log approximation in simulating Quantum Chromodynamic events is described. Models for the formation of hadrons from quarks and gluons are reviewed. A model for hadron hadron scattering, using the leading log approximation and a particular model for hadron formation is described. This model is used to study the results of calorimetric experiments.

## **Acknowledgment**

I thank the many people whose help has made this work possible. I thank the members of the Caltech high energy physics group for helpful discussions. I particularly thank H. D. Politzer and R. P. Feynman for many helpful discussions. I learned much of what I know about QCD from classes taught by R. D. Field and R. P. Feynman.

T. D. Gottschalk gave me invaluable help in understanding and using the QCD cluster model, and offered many helpful suggestions about the text of this thesis.

I thank my advisor, G. C. Fox, for his encouragement and support, many helpful discussions, and good advice.

I thank my parents for their love and support. I am very grateful to my wife Lisa for her love and support, and for the many sacrifices, both personal and financial, she made to enable me to pursue my studies.

**Table of Contents**

1. Introduction .....	1
References .....	6
2. The Leading Log Approximation to QCD .....	7
2.1 Introduction .....	7
2.2 Derivation and simplification of the spin sum .....	9
2.3 Explicit formulae for the density matrices .....	16
2.4 Quark helicities .....	19
2.5 Use of leading log approximation in Monte Carlo programs .....	21
References .....	25
3. Hadronization Models .....	26
3.1 Independent fragmentation—the Field Feynman model .....	26
3.2 String models—the Lund model .....	28
3.3 Cluster models .....	32
References .....	35
4. Event Generation in Hadron Hadron Scattering .....	37
4.1 Introduction and overview .....	37
4.2 Choosing the initial partons .....	39
4.3 The evolution to the scale $Q^2$ .....	43
4.4 Hard scatter and cross section .....	48
4.5 Parton evolution after the hard scatter .....	50
4.6 Formation of the clusters .....	51
4.7 The beam remnants .....	53
4.8 Hadronization .....	57
References .....	59

5. Comparison of the Model with Experiment .....	60
References .....	69
Figures for Chapter 5 .....	70
6. Discussion and conclusions .....	87
6.1 Areas of phenomenological concern.....	87
6.1.1 Treatment of gluons .....	87
6.1.2 The beam remnant .....	88
6.2 Other concerns.....	90
6.2.1 Better perturbative approximations .....	90
6.2.2 Cutoffs and a spacetime picture.....	91
6.3 Conclusions.....	92
References .....	93
Appendix—Use of the Monte Carlo Program.....	94

## 1. Introduction

It is now widely believed that Quantum Chromodynamics (QCD) is the correct theory of the strong interactions<sup>1</sup>. This theory describes the dynamics of quarks and gluons, collectively called partons, which are pointlike constituents of hadrons. The quarks are spin  $1/2$  particles that undergo an interaction mediated by the gluons, which have spin 1. QCD is asymptotically free<sup>2</sup>, that is the interaction is strong at large distances; i. e., small momentum transfers, and becomes weak at short distances, i. e., large momentum transfers. This means that the short distance behavior of the theory can be calculated perturbatively, while the large distance behavior, which includes the binding of partons into hadrons, cannot. It is believed that one consequence of QCD is that colored objects cannot be separated by large distance<sup>3</sup> (compared to hadron radii). Thus, quarks and gluons are permanently confined to the interior of hadrons. This property is called confinement. Because QCD confines its basic quanta, the quarks and gluons, they are never seen in particle detectors, which detect the hadrons made up of partons. Although some progress is being made in the calculation of hadronic properties using the techniques of lattice gauge theory<sup>4</sup>, there are, as yet, no reliable calculations of the predictions of QCD for the properties of hadrons. However, because of the asymptotic freedom of QCD we can hope to use high energy experiments as probes of the dynamics of partons and as tests of QCD.

It is, however, not so easy to compute the predictions of the theory. Any experimental process involving hadrons always has some soft, i. e., long distance, physics; at the very least, it will depend on the properties of the hadrons involved. While there are some observables for which this dependence is not very important, there are many observables of interest for which this is not the case. To calculate QCD predictions for these processes one must include some

phenomenological model describing the binding of partons into hadrons in addition to perturbative calculations of the hard, that is, short distance, processes which may be involved.

QCD predictions that are not sensitive to the soft physics are in rough agreement with the data. These include the ratio of the cross sections for  $e^+e^-$  annihilation to muon pairs and hadrons<sup>5</sup>, ratios of total inclusive cross sections in neutrino-nucleon and muon-nucleon scattering, the approximate scaling of deep inelastic structure functions at high momentum transfer, and its violation<sup>6</sup>. Most of these tests require data that are very difficult to measure accurately. At the level of accuracy currently achieved these experiments tend to test the existence of quarks that have the quantum numbers expected from QCD and that interact weakly at the high energy scales probed. Accurate tests of the dynamics of the partons are not at present available. QCD based models, typically involving *ad hoc* assumptions about the long distance behavior of quarks and QCD predictions for their short distance behavior, have been successful in explaining the spectrum of hadrons<sup>7</sup>. Preliminary calculations using lattice QCD indicate that the bound states of QCD are the hadrons observed experimentally<sup>4</sup>, but these are not yet accurate enough to provide a quantitative test of the theory.

It has recently been claimed that that jet cross sections at collider energies<sup>8</sup> and an asymmetry in an energy energy correlation<sup>9</sup> are tests of QCD that are insensitive to the soft physics. It remains to be seen whether or no these claims become generally accepted.

In this thesis we shall consider observables that are sensitive to the soft physics. Most experimental observables fall into this class. While we shall not be able to test QCD using these models, without having to deal with model

dependent effects, we will be able to consider a wider variety of experiments, most of which are more accurate than those for which clean calculations are possible. We shall also be able to probe aspects of QCD that are not tested by the cleanly calculable observables, like the behavior of gluons. We can also try to learn about the behavior of QCD at larger distances by analyzing the comparison of experiment to the models.

We should keep in mind two closely related, long term goals of the investigation of hadronization models. One is to develop an understanding of the hadronization process; the other is to develop a model sufficiently reliable that one believes its predictions for some of the observables sensitive to the soft physics.

Two experimental processes that we shall consider in detail are high energy  $e^+e^-$  annihilation to hadrons, and high  $E_T$  hadron hadron scattering. The QCD description of the former is that the electrons annihilate to a virtual photon which decays into a quark antiquark pair, which may, in turn, radiate gluons and quark antiquark pairs. These partons eventually form hadrons. The formation of the initial quarks and the radiation of hard partons from them can be calculated from QCD by perturbative methods. The formation of the hadrons from the partons must be described by some phenomenological model.

In high  $E_T$  hadron hadron scattering, two hadrons scatter, forming a system of hadrons with a high value of transverse energy,  $E_T$ , i. e.,  $\sum E_i \sin\vartheta_i$ , where  $E_i$  is the energy of the  $i^{th}$  particle and  $\vartheta_i$  is the angle between the momentum of the  $i^{th}$  particle and the beam axis, all measured in the center of mass frame. The sum is over all particles in the final state. The QCD description of this process is that two partons, one from each of the incoming hadrons, undergo a hard collision, each having, possibly, radiated some partons before the hard collision. The resulting partons then form hadrons. Here, the hard collision and radiation can

be calculated perturbatively; the formation of hadrons from the partons and the momentum distribution of the partons in the original hadrons must be modeled phenomenologically.

A useful and common method for calculating QCD predictions for experimental observables is to generate simulated events according to the predictions of QCD and the phenomenological model for the soft physics. This approach is needed because the phenomenological model for the formation of hadrons typically gives statistical distributions for the number, types, and momenta of the hadrons generated from some partons that are sufficiently complicated that analytic calculations are not possible. These event generation programs are also useful for the analysis of experimental apparatus.

This thesis discusses an event generator that uses the QCD cluster model to describe the formation of the hadrons. We believe that this is the most theoretically sound model yet proposed. The perturbative calculations on which the event generator relies are developed and discussed, and the QCD cluster model is described in detail and compared with other models. The algorithm of the event generator is discussed in detail. The event generator is used to study hadron hadron scattering, and its predictions are compared with experiment. The agreement is generally good, but there are some discrepancies. These point out a weakness of the version of the QCD cluster model; there is discussion of improvements to the model that will correct this. Work toward implementing these improvements is in progress.

In chapter 2 of this thesis we shall develop an approximation to the QCD predictions for hard radiation that is particularly well suited for statistical event generation. Chapter 3 contains a discussion of models for the formation of hadrons from collections of partons. Chapter 4 is a detailed discussion of an

event generator for high  $E_T$  hadron hadron scattering. Chapter 5 is a discussion of the predictions of the model of chapter 4, including comparisons with experimental data. Chapter 6 discusses the results of the studies, presents some conclusions and suggest some possible improvements to the model, some of which are currently under investigation. A detailed description of the use of the program described and used in this thesis is presented as an appendix.

### References for Chapter 1

- [1] H. D. Politzer, Talk presented at 21st Int. Conf. on High Energy Physics, Paris, France, Jul. 26-31, 1982.  
F. Eisele, Dortmund University preprint DO-EXP-82/5, Invited talk given at 10th Int. Winter Mtg. on Fundamental Physics and 13th GIFT Int. Seminar on Theoretical Physics, Masella, Spain, Jan. 28-Feb. 6, 1982.
- [2] H. D. Politzer, *Phys. Rep.* **14C** (1974) 129.
- [3] E. T. Tomboulis, *Phys. Rev. Lett.* **50** (1983) 885.
- [4] M. Creutz, L. Jacobs and C. Rebbi, *Phys. Rep.* **95C** (1983) 201.
- [5] E. Hilger, Invited talk given at 5<sup>th</sup> International Conference, "Novel Results in Particle Physics," Vanderbilt Univ., Nashville, Tennessee, May 24-26, 1982.
- [6] By H.E. Montgomery, CERN preprint CERN-EP/82-164, Lectures given at 1982 Arctic School of Physics: Gauge Theories of the Eighties, Akaslompolo, Finland, Aug 1-13, 1982.
- [7] T.A. DeGrand, R. L. Jaffe, K. Johnson, and J. Kiskis, *Phys. Rev* **D15** (1977) 281.
- [8] W. Furmanski and H. Kowalski, *Nucl. Phys.* **224** (1983) 523.
- [9] B. Adeva, *et al.*, *Phys. Rev. Lett.* **50** (1983) 2051.

## 2. The Leading Log Approximation to QCD

### 2.1. Introduction

As we have mentioned, a useful method for computing the predictions of QCD for some observables is to simulate events using perturbative QCD to describe the hard scattering of partons, and using some QCD based model to describe the combination of partons into hadrons. In this chapter we shall discuss the perturbative part of the calculation.

It can be advantageous not to use the full perturbative cross sections to some order in the coupling constant to describe the probability for a particular parton final state; it is often preferable to use an approximation to the probability at each order in the coupling. This is for two reasons: at high energy parton final states with many partons are important — it would be too difficult to compute the perturbation series to a high enough order — and the complexity of the hadronization calculations and the structure of the perturbative probabilities make it desirable to produce parton final states distributed according to the probabilities rather than to generate the parton final states uniformly, and then weigh them by the perturbative probability. Because the probability for the parton final state is singular as the partons become on shell and collinear, most of the uniformly generated events would have low weight; much time would be spent computing the hadron final states coming from unimportant parton final states.

In this chapter we shall discuss a particularly useful approximation for this purpose, and its application in the parton shower calculations used in event generators. The approximation we shall use is to consider only the part of the perturbative probability that is most singular in the collinear limit, to the lowest

order in  $\alpha_s$  possible for the particular parton state, the so-called leading log approximation. This approximation is very easy to calculate for any parton final state. Because, in an axial gauge, there is no interference between diagrams, in the leading log approximation, it is easy to generate parton final state with the leading log approximation distribution by a shower Monte Carlo. One begins with some collection of partons; any one of them has a certain probability of radiating, leaving a new system with one more parton. One can continue in a recursive fashion until there are no more partons that will decay. Because the leading log approximation can be described without interference effects, we can say that a parton resulted from the decay of a particular other parton, so we can construct a decay tree as described above. A shower Monte Carlo<sup>1-3</sup> uses the lack of interference to generate the parton final state recursively. The initial partons are generated from the decay of the virtual photon (in  $e^+e^-$ ); they each have a definite probability to be in the parton final state and probabilities for various decays. The partons produced in these decays, in turn, may be in the parton final state or may decay again, and so on. One can then weigh the events generated according to the leading log approximation by the ratio of the most accurately known value for the parton level cross section to the leading log approximation. The weights would be much more uniform for the events distributed according to the leading log approximation than they would be for uniformly distributed events.

The Monte Carlo programs now in use<sup>1</sup> do not use the correct leading log approximation probabilities. In these calculations the vertices are treated as though the amplitude for a decay were independent of the partons' polarizations. Even in the leading log approximation this is not true. The difference between the amplitudes for different polarizations introduces a correlation

between the plane in which a gluon is produced and that in which it decays. For observables that depend on the spins of the particles in the final state, it is, of course, necessary to treat the polarizations correctly.

We shall derive the leading collinear singularity (leading log approximation), discuss a simplified version for the common case where the observables do not depend on the spins of the particles. We shall then discuss the use of the leading log approximation in parton shower event generators. Throughout this chapter we shall consider processes for which there are no partons in the initial state, canonically  $e^+e^-$  annihilation to hadrons; the extension to processes with initial state partons will be discussed in chapter 4.

## 2.2. Derivation and simplification of the spin sum

In an axial gauge (defined by  $\eta \cdot A = 0$  for some fixed vector  $\eta$ ) the leading log approximation to an exclusive amplitude is, as is shown below, the sum of squares of tree graphs<sup>†</sup>. We can compute such a graph by a simple procedure that we describe below.

An arbitrary tree graph can be written as the product of vertices, propagators, and external wave functions. For instance, the graph of Fig. 1 is usually written as (We neglect color factors here and in most of the chapter; they are included in the final formulae for the density matrices.):

---

<sup>†</sup> There are some (infrared singular) loop diagrams that contribute to the leading log approximation. Some give the running of the coupling constant; others cancel soft divergences in the tree graphs. This is, for the moment, an inessential complication; we shall return to this question at the end of the chapter when we discuss leading log approximation showers.

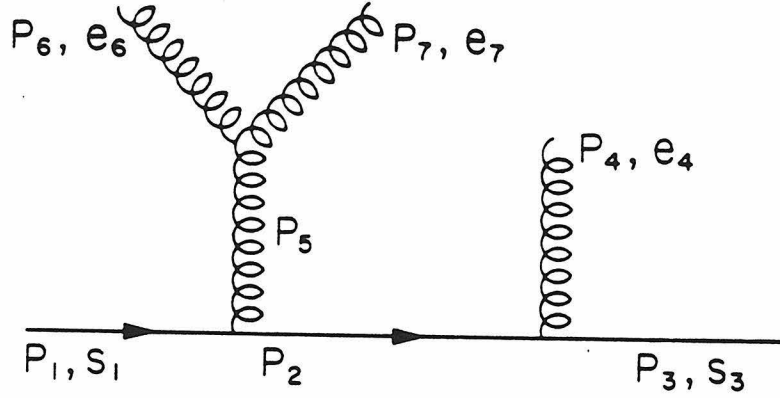


Fig. 1

$$\begin{aligned}
 & \bar{u}(p_3, s_3) \gamma_{\mu_4} \frac{\not{t}_2}{t_2} \gamma^{\mu} u(p_1, s_1) \frac{g_{\mu\nu}}{t_5} \\
 & \times (P_5 - P_6)_{\mu_7} g_{\mu_6 \nu} + (P_6 - P_7)_{\nu} g_{\mu_6 \mu_7} + (P_7 - P_5)_{\mu_6} g_{\nu \mu_7} \\
 & \times e_4^{\mu_4} e_6^{\mu_6} e_7^{\mu_7}.
 \end{aligned} \tag{2.1}$$

(Of course not all the momenta above are independent.)  $G_{\mu\nu}/t_5$  is the axial gauge propagator for the gluon, and  $\not{t}_2/t_2$  is the propagator for the quark. ( $t_i = p_i^2$ ). The spin sum  $G_{\mu\nu}$  is given by:

$$G_{\mu\nu} = -g_{\mu\nu} + \frac{\eta_{\mu} k_{\nu} + \eta_{\nu} k_{\mu}}{\eta \cdot k} - \frac{\eta^2 k_{\mu} k_{\nu}}{(\eta \cdot k)^2}. \tag{2.2}$$

Throughout this chapter the current masses of the quarks are neglected; when the mass of a parton is mentioned, the square root of the square of the four momentum is meant. At the end of the chapter we shall discuss the question of massive quarks. The (explicitly written)  $\gamma$  matrices and the portion in bold face are the three vertices. The spinors  $u$  and vectors  $e$  are the external wave functions.

The propagator for any line can be written as:

$$P_{\alpha\beta} = \sum_{\text{spins } s} f(s) \frac{\varphi_{\alpha}(s) \bar{\varphi}_{\beta}(s)}{t}, \quad (2.3)$$

where  $\varphi$  is a wave function (either a spinor or vector) of the momentum of the line,  $\alpha$  and  $\beta$  are indices of the appropriate type, and  $t$  is the square of the momentum four vector. This spin sum is not only over the physical spins of the on shell particles, but over the possible spins for the off shell particles. For the gluons this means there are spin 0 and spin 1, helicity 0 components. For the fermions the spin sum must include spinors of both parities, that is, the positive energy spinors of the (three) momentum of the line, and the negative energy spinors of the negative of this momentum.  $f(s)$  is a weight. It is  $\pm 1/2$  for the fermions, 1 for the helicity  $\pm 1$  gluons, and something that goes to zero with the mass for the other gluon spin states. The vertices are functions of the momenta coming into the vertex, and have indices on which to contract the wave functions for the particles coming into the vertex. We can define a "capped vertex" to be a vertex with wave functions contracted in; it is a function of the momenta and spins of the incoming particles.

For a three-gluon vertex the capped vertex is:

$$\begin{aligned} \tilde{V}(\mathbf{p}, \mathbf{p}_1, \mathbf{e}, \mathbf{e}_1, \mathbf{e}_2) = & \mathbf{e} \cdot (\mathbf{p}_1 - (\mathbf{p} - \mathbf{p}_1)) \mathbf{e}_1 \cdot \mathbf{e}_2 + \mathbf{e}_1 \cdot ((\mathbf{p} - \mathbf{p}_1) + \mathbf{p}) \mathbf{e} \cdot \mathbf{e}_2 \\ & + \mathbf{e}_2 \cdot (-\mathbf{p} - \mathbf{p}_1) \mathbf{e} \cdot \mathbf{e}_1, \end{aligned} \quad (2.4)$$

where  $\mathbf{p}$  is the momentum of the incoming gluon, and  $\mathbf{e}$  is its polarization;  $\mathbf{p}_1$  is the momentum of an outgoing gluon with polarization  $\mathbf{e}_1$ , and  $\mathbf{e}_2$  is the polarization of the other outgoing gluon. If the polarizations are orthogonal to the corresponding momenta, as the ones for physical helicity states are, this simplifies to:

$$\tilde{V}(\mathbf{p}, \mathbf{p}_1, \mathbf{e}, \mathbf{e}_1, \mathbf{e}_2) = 2\mathbf{e} \cdot \mathbf{p}_1 \mathbf{e}_1 \cdot \mathbf{e}_2 + 2\mathbf{e}_1 \cdot \mathbf{p} \mathbf{e} \cdot \mathbf{e}_2 - 2\mathbf{e}_2 \cdot \mathbf{p} \mathbf{e} \cdot \mathbf{e}_1. \quad (2.5)$$

The capped vertex for a  $q \rightarrow qG$  vertex is:

$$\bar{u}(p-k, s_f) \not{\epsilon} u(p, s_i), \quad (2.6)$$

where the  $s$ 's are spins,  $\epsilon$  is the gluon polarization,  $p$  is the momentum of the incoming quark,  $k$  is the (outgoing) gluon momentum, and  $u$  is a spinor. A general tree graph can be written as the sum over all internal spins of a product of capped vertices and a factor of  $1/t_i$  for each internal line. Of course, the spin of a particular internal line is the same for the vertices at the two ends of the line.

Using the capped vertices we can write the graph of Fig. 1 as:

$$\sum_{s_2 s_5} \frac{f(s_2) f(s_5)}{t_2 t_5} \tilde{V}(p_1, p_2, s_1, s_2, s_5) \tilde{V}(p_2, p_3, s_2, s_3, s_4) \tilde{V}(p_5, p_6, s_5, s_6, s_7), \quad (2.7)$$

where the spin sum is as in Eq. (2.1), and the  $\tilde{V}$  are the capped vertices. The capped vertices have dimensions of mass. We shall show below that, if one restricts the gluon polarizations to those that propagate in an axial gauge, the leading behavior of the capped vertices as all the partons go on shell is proportional to the masses of the partons. If we did not restrict the polarization of the gluons, we would have terms in the capped vertices that were proportional to the energy of the decaying parton in the lab frame; they would cancel among different graphs. This is why the leading log approximation includes interference among graphs in a covariant gauge. In an axial gauge any interference term would go like, at most,  $1/\sqrt{t_1 t_2}$ . If one were interested in an observable that does not depend on the momentum of the partons in question, say a single particle inclusive cross section, the leading log approximation has a nonintegrable singularity, where the interference term has two integrable singularities. The kinematics constrains the mass of a child parton to be less than that of its parent<sup>1</sup>. Since we are interested in the leading behavior as the masses of the internal lines becomes small we shall neglect the terms in any capped vertex

that are proportional to  $M_{chud}$ , the mass of an outgoing parton.

The sum over spins for the internal lines can be greatly simplified. It is shown below that leading parts of the capped vertices are indeed proportional to the parton masses, and that the unphysical helicities of the gluon decouple in the leading log approximation. We shall also show that we can replace the sum over 4 spinors for each fermion propagator with a single spinor times its Dirac conjugate. This means that the sum over 4 spins for each internal line can be reduced to a sum over 2 spins for each gluon line; no spin sum is needed for the internal quark lines.

We shall use an axial gauge whose gauge vector  $\eta$  is time-like and future directed (so that it is not orthogonal to the four momentum of any gluon) and not equal to the four momentum of any gluon.<sup>†</sup> In such a gauge the polarization of the spin zero gluon is proportional to  $k^\mu$ , and that of the helicity 0, spin 1 gluon, to  $(\eta \cdot k)k^\mu - (k \cdot k)\eta^\mu$ , where  $\eta$  is the gauge vector. Polarizations along  $\eta$  do not propagate, since  $G_{\mu\nu}\eta^\nu=0$  so if the spin 0 gluons do not contribute to the leading log approximation, the spin 1, helicity 0 ones don't do so either. Since the spin 0 gluons are polarized along their four momentum, we shall call them longitudinal.

We begin with the **qqG** vertices. These capped vertices are functions of two independent momenta, the spin of the gluon, whether the spinors are positive or negative energy solutions, and the helicities of the two quarks. Because of the vector nature of the vertex, the capped  $q \rightarrow qG$  vertex is zero if the helicities of the quarks are not the same. The  $G \rightarrow q\bar{q}$  capped vertex is zero if the helicities

---

<sup>†</sup>The gauge whose gauge vector is along the direction of the virtual photon is an example of such a gauge. The lightlike gauge chosen by Odorico (Ref. 2) is, in the collinear limit, along the four momenta of all the partons in one jet so it does not fit into this class.

are not opposite. Since the propagator for massless fermions also conserves helicity, from a knowledge of the helicities of the external quarks the helicity of each internal quark line can be determined. The vertex conserves total helicity in the collinear limit, so the capped vertex for helicity  $\pm 1$  gluons is of order of the largest mass, that is,  $M_{parent}$ . Because of current conservation, the longitudinal gluons do not couple to on shell quarks; the capped vertex is of order of the mass of the more off shell quark.

We can,<sup>2</sup> in the leading log approximation, replace the factor  $\not{p}$  in the numerator of a quark propagator with  $\not{p}_1$ , where  $p_1 = p - (p \cdot p)v / (2v \cdot p)$ , where  $v$  is any fixed vector whose dot product with  $p$  does not vanish as  $p \cdot p$  goes to zero. This changes the spin sum by a term of order  $p \cdot p$ , but we are neglecting anything smaller than  $\sqrt{p \cdot p}$  anyway. The vector  $p_1$  is, to order  $(p \cdot p)^2$ , light-like. Therefore we can write  $\not{p}_1$  as  $\sum_{spins} u(p_1, s) \bar{u}(p_1, s)$ ; the sum is now only over the positive energy spinors. The spinor that has a definite helicity with the momentum  $p_1$  is, up to corrections of order  $(p \cdot p)$ , a linear combination of the positive and negative energy spinors of momentum  $p$  and the same helicity, so the discussion about helicity conservation above is still valid. The difference between these spinors is of order  $\sqrt{(p \cdot p)}$ , so when the spinor represents a child quark this difference can be ignored. When we give explicit forms for the capped vertices we shall use the spinors with the choice  $v = \eta$ , the gauge vector. This is a matter of convenience; other choices differ by subleading terms. We have replaced a sum over 4 spinors for each fermion propagator with a single spinor times its Dirac conjugate. If we have an observable that is insensitive to the helicity of the final state fermion, we must sum over the helicities of each fermion line, rather than those of each fermion propagator. In fact, we can do this sum easily for any graph; as is discussed in section 4, the quark-gluon density

matrices are replaced by their helicity averages.

The three-gluon vertex also conserves helicity in the collinear limit, even though it is momentum dependent. Because of current conservation, the longitudinal gluons do not couple to on shell gluons of physical helicity ( $\pm 1$ ). The capped vertex coupling three longitudinal gluons also vanishes in the collinear limit because the coupling is  $(k_\mu A_\nu - k_\nu A_\mu)[A_\mu, A_\nu]$ . Since both factors in the coupling vanish for three collinear longitudinal gluons, this capped vertex is of order of the square of the largest mass. These facts imply that all three-gluon capped vertices vanish in the collinear limit; the capped three-gluon vertices are, at most, of order  $M_{parent}$  whether the gluons be longitudinal or of physical spin. Since the propagation of longitudinal gluons is suppressed by the factor  $f$  of Eq. (2.3), which vanishes with the mass of the line, they do not contribute to leading log approximation.

Each capped vertex is of order  $M_{parent}$ . We can write the square of a tree graph as the sum over the spins of the internal gluons of the product of a factor  $1/t^2$  for each internal line, and for each vertex, a capped vertex times the complex conjugate of a capped vertex (in general with different spins for the gluons). The product of the two capped vertices is  $t_{parent}$  times a function of the spins of the (two or six) gluons; we shall call this function a density matrix, since its properties and significance are very much like those of a density matrix.

There are two independent possibilities for each gluon spin. We can write the quark-gluon density matrices as  $2 \times 2$  matrices and the three-gluon density matrix as a  $2 \times 2 \times 2 \times 2 \times 2 \times 2$  matrix, the indices running over the values of the gluon spins. The sum over gluon spins becomes a trace of the products of density matrices over the relevant indices. Thus, (square of) the graph of Fig. 1 represents a probability of

$$\frac{\rho_{q \rightarrow G}^{jj'}(z_5) \rho_{q \rightarrow G}^{kk}(z_4) \rho_{G \rightarrow GG}^{jj' \rightarrow ll+mm}(z_6)}{t_2 t_5}. \quad (2.8)$$

The  $\rho$ 's are the density matrices, the  $t_i$  are the mass-squareds of the decaying particles, and repeated indices are summed over. The density matrices depend only on the variable  $z$ , which is something that approaches the momentum fraction of the child particle in the collinear limit. This criterion does not specify  $z$  uniquely; different choices for  $z$  differ by subleading terms. Converting the basis at the production of a gluon to the basis at its decay introduces a dependence on the angle between the production planes.

### 2.3. Explicit formulae for the density matrices

The basis in which the density matrices are most simple is related to the so-called "transversity" basis, that is, the basis whose states are the eigenstates of the component of gluon spin perpendicular to the production plane. The antisymmetric combination of the "transversity" +1 and "transversity" -1 states is the helicity 0 state, and is not present in leading log approximation. Our two basis states will be the "transversity" 0 state, which we call state 1, and the symmetric combination of "transversity" +1 and -1, which we call state 2. In this basis the density matrices are:

$$\rho_{q \rightarrow qG}^{ii'}(z) = \frac{4}{3} g^2 \begin{bmatrix} z & -2ih(2-z) \\ 2ih(2-z) & z + \frac{4(1-z)}{z} \end{bmatrix} \quad (2.9a)$$

where  $z$  is the momentum fraction of the gluon and  $h$  is the helicity of the quark ( $\pm \frac{1}{2}$ ).

$$\rho_{G \rightarrow q\bar{q}}^{ii'}(z) = g^2 \begin{bmatrix} 1/2 & ih(1-2z) \\ -ih(1-2z) & 1/2 - 2z(1-z) \end{bmatrix} \quad (2.9b)$$

where  $z$  is the momentum fraction of the quark and  $h$  its helicity ( $\pm \frac{1}{2}$ ), and

$$\rho_{G \rightarrow GG}^{ii' \rightarrow jj' + kk'} = 6g^2 \left( \delta^{i'2} \delta^{jk} \sqrt{z(1-z)} - \delta^{ik} \delta^{j'2} \sqrt{\frac{1-z}{z}} - \delta^{k'2} \delta^{ij} \sqrt{\frac{z}{1-z}} \right) \quad (2.9c)$$

$$\left( \delta^{i'2} \delta^{j'k'} \sqrt{z(1-z)} - \delta^{i'k'} \delta^{j'2} \sqrt{\frac{1-z}{z}} - \delta^{k'2} \delta^{i'j'} \sqrt{\frac{z}{1-z}} \right),$$

where  $z$  is the momentum fraction of the gluon whose spin is represented by the indices  $j$  and  $j'$ . These density matrices can be understood by considering the operation of a spatial inversion, followed by a rotation of  $\pi$  about the normal to the plane of the vertex. This is a symmetry of the density matrix. Those elements that would change sign under this operation (which leaves "transversity" unchanged and reverses helicity) are precisely those that are zero. This symmetry is also why the off-diagonal elements of the quark density matrices are the ones proportional to the helicity. A vertex, for a particular quark helicity, can be viewed as a vector in the two-dimensional space of gluon spins. The density matrix for a particular helicity of quark is thus of the form  $vv^\dagger$ , where  $v$  is the vector representing the vertex; this is why the density matrices of Eqs. (2.9a) and (2.9b) have zero eigenvalues.

We can use these results to write the probability for the graph of Fig. 1. It is:

$$\left( \frac{8}{3}g^2 \right) (6g^2) \left( \frac{4}{3}g^2 \right) \left[ \frac{1+(1-z_4)^2}{z_4} \right] \times \quad (2.10)$$

$$\left\{ 2 \frac{(1-z_6+z_6^2)^2}{z_6(1-z_6)} \frac{1+(1-z_5)^2}{z_5} + 2z_6(1-z_6) \frac{1-z_5}{z_5} \cos 2\varphi \right\},$$

where  $\varphi$  is the angle between the plane defined by  $\vec{p}_1$  and  $\vec{p}_2$  and that defined by  $\vec{p}_6$  and  $\vec{p}_7$ . The term in curly braces is the contraction of the two density matrices involving the virtual gluon. The  $\varphi$  dependence occurs because the gluon is more likely to be emitted polarized in the production plane, that is in state 2; and it is more likely to decay into the plane defined by its polarization

and momentum.

The formula for the leading log approximation to the square of a graph can be expressed recursively. Suppose  $A_N^{i_1 i'_1 \dots i_m i'_m}$  is the leading log approximation to the density matrix for a graph with  $m$  gluons and  $N-m$  quarks in the final state. The indices correspond to the spins of the  $m$  gluons in the final state. The probability corresponding to this graph, if the observable does not depend on the gluon spins, is:

$$A_N^{i_1 i'_1 \dots i_m i'_m} \delta^{i_1 i'_1} \dots \delta^{i_m i'_m}, \quad (2.11)$$

If we were interested in an observable that depended on the gluon spins, we would replace the Kronecker  $\delta$ 's of Eq. (2.10) with a matrices corresponding to a suitably weighted spin sum. Now we consider a graph generated when one of the final state partons of this graph radiates. There are three possibilities: a quark can radiate a gluon, a gluon can decay into two gluons, and a gluon can decay into a  $q\bar{q}$  pair. If a quark radiates, the new density matrix is:

$$A_{N+1}^{i_1 i'_1 \dots i_{m+1} i'_{m+1}} = A_N^{i_1 i'_1 \dots i_m i'_m} \frac{\rho_{q \rightarrow qG}^{i_{m+1} i'_{m+1}}(z)}{t}, \quad (2.12)$$

where  $t$  is the off shell mass of the decaying quark and  $z$  is the momentum fraction of the decay. Since we neglect the dependence of the density matrices on the child masses, we use the  $A_N$  with the decaying parton on shell; this is also true for the other cases below. If a gluon, say the  $m^{\text{th}}$ , decays to a  $q\bar{q}$  pair, we would have:

$$A_{N+1}^{i_1 i'_1 \dots i_{m-1} i'_{m-1}} = A_N^{i_1 i'_1 \dots i_m i'_m} \frac{\rho_{G \rightarrow q\bar{q}}^{i_m i'_m}(z)}{t}. \quad (2.13)$$

The repeated indices are summed over. Finally if a gluon, say gluon 1, decays into two gluons, we would have:

$$A_{N+1}^{i_2 i_2' \dots i_{m+2} i_{m+2}'} = A_N^{i_1 i_1' \dots i_m i_m'} \frac{\rho_{G \rightarrow GG}^{i_1 i_1' \dots i_{m+1} i_{m+1}' i_{m+2} i_{m+2}'}(z)}{t}. \quad (2.14)$$

For all three cases one computes the probability by tracing over the spin of each gluon in the final state. The density matrices are given above in Eq. 2.9; if we are considering an observable independent of the quark helicities we can replace  $\rho_{q \rightarrow qG}^{ii'}$  and  $\rho_{G \rightarrow q\bar{q}}^{ii'}$  with their helicity averages, as is shown below. Finally, if one is to generate properly distributed events, he needs to know the phase space for each vertex, which is:

$$\frac{1}{8\pi^2} dt dz \frac{d\varphi}{2\pi}, \quad (2.15)$$

where  $t$  is the mass squared of the decaying parton,  $z$  the momentum fraction carried by one of the children, and  $\varphi$  is an azimuthal angle.

#### 2.4. Quark helicities

If one were to consider a single particle inclusive observable that does not depend on parton spins, like the  $Q^2$  dependence of a fragmentation function, one would trace over all spins. This is because when we sum over all possibilities for the other particles, each particle is equally likely to have either helicity. If one does so to the above density matrices, he recovers the famous result of Altarelli and Parisi<sup>4</sup>. In the Monte Carlo programs currently in use,<sup>1</sup> the correct density matrices are replaced by the Altarelli-Parisi splitting functions. This destroys the correlation between the production plane of a gluon and its decay plane, which is present in the correct leading log approximation result. This effect is not very important, as the coefficient of the azimuthal dependence coming from a  $G \rightarrow GG$  decay has a coefficient that vanishes at the points where the splitting function is singular; see, for example, Eq. 2.10. The  $G \rightarrow q\bar{q}$  decay is unimportant, as gluons almost always decay into gluons.

If the observable one were interested in were independent of the helicity of the final state particles, one can replace each quark density matrix with its average over helicities, which achieves a further simplification. We prove that this can be done by a recursive argument based on the antisymmetry, in our basis, of the helicity dependent part of the  $q \rightarrow Gq$  density matrix. We shall work from the bottom of the tree up, that is, starting from the final partons. If we contract a symmetric matrix into a  $q \rightarrow qG$  density matrix, the result is independent of helicity, so we can replace by its helicity average any  $q \rightarrow qG$  density matrix that is contracted into a symmetric matrix. If we symmetrize  $\rho_{G \rightarrow GG}^{ii' \rightarrow jj'kk'}$  with respect to  $j$  and  $j'$  and with respect to  $k$  and  $k'$ , the result is symmetric in the variables  $i$  and  $i'$ . Finally, if all the  $q \rightarrow qG$  density matrices on a particular quark line have been replaced by their helicity averages, one can replace the  $G \rightarrow q\bar{q}$  density matrix on this line by its helicity average, since it is now the only density matrix to depend on the helicity of that line. We begin by replacing the  $G \rightarrow q\bar{q}$  density matrix for any gluon decaying into final state quarks by its helicity average. We proceed recursively as follows. Consider a  $q \rightarrow qG$  vertex such that all the descendants of the gluon are either gluons or quarks such that the density matrices on the quark line have all been replaced by their helicity averages. Since all the density matrices below the gluon are symmetric, the matrix contracted into the density matrix for this vertex is symmetric, so the density matrix can be replaced by its helicity average. Next, replace the density matrix for each  $G \rightarrow q\bar{q}$  vertex such that all the  $q \rightarrow Gq$  density matrices on that quark line have been replaced by their helicity averages with its helicity average. If there are any quark lines left whose density matrices have not been replaced by their helicity averages, the process is repeated. Each recursion replaces the all density matrices on at least one quark line with their helicity averages, so only a finite number of steps are needed.

That one can replace the  $q \rightarrow Gq$  density matrix under the conditions described above with its helicity average, follows from the charge conjugation invariance of the strong interactions. Charge conjugation reverses the helicity of a spinor, and does not affect the gluons. Therefore, the dependence of the  $q \rightarrow Gq$  density matrix, contracted over the part representing the descendants of the gluon, can depend on the quark helicity only through its product with the helicity of some quark descended from the gluon. (Since that contracted density matrix is a permissible strong interaction graph, and in the leading log approximation there is no interference between graphs, it must be charge conjugation invariant). This means that if the product of density matrices representing the descendants of the gluon doesn't depend on any quark helicity, the contracted density matrix for the  $q \rightarrow Gq$  vertex doesn't depend on the helicity of the decaying quark. Note that, even if we don't average over final state helicities, the leading log amplitude depends only on the helicities of quark lines that radiate gluons that in turn decay into quarks and those of these descendant quarks.

## 2.5. Use of leading log approximation in Monte Carlo programs

One can generate parton final states distributed according to the the leading log approximation by a Monte Carlo procedure<sup>†</sup>. To do so one must address the issue of the singularities of the density matrices as the 4-momentum of a gluon goes to zero. Formally, these are canceled by a  $\delta$  function with an infrared singular coefficient that comes from graphs with vertex and self-mass corrections in place of the emission. To deal with this one needs an infrared cutoff. We shall follow Ref. 3 in demanding that  $z$  be such that it would be

---

<sup>†</sup> The discussion in the beginning of this section follows that of Ref. 3.

consistent with both daughter partons' being on shell.

We shall begin by considering a single parton; the behavior of systems of partons is determined by decaying each of the partons in the system recursively, until no parton decays further before the cutoff. Kinematically the mass of a parton must be less than the mass of its parent, that is, the parton whose radiation gave rise to it. The probability that the parton doesn't radiate between the maximum  $mass^2$ ,  $t_{\max}$ , and some  $mass^2$ ,  $t$  is

$$P \equiv \Pi(t_{\max}, t) = \left( \frac{\log(t/\Lambda^2)}{\log(t_{\max}/\Lambda^2)} \right)^{\gamma/b}, \quad (2.16)$$

where,

$$b = 11/2 - 1/3n_f. \quad (2.17)$$

$\gamma$  is

$$\gamma = \int P(z) dz, \quad (2.18)$$

where  $P$  is the Altarelli-Parisi splitting function. The integral is over those values consistent with the cutoff. This is actually an underestimate; it is based on the cutoff's being independent of the mass of the decaying parton. The allowed range of  $z$  contracts as the mass of the decaying parton increases. The procedure described below will distribute the masses correctly. We begin, assuming the parton has been determined to decay between  $t_{\max}$  and  $t_{cut}$ , a resolvability cut, according to Eq. 2.16, by choosing a  $mass^2$  according to the probability distribution

$$\frac{dP}{dt} = \frac{\Pi(t_{\max}, t) \alpha_s(t) \gamma}{2\pi t} dt. \quad (2.19)$$

Having chosen a value of the  $mass^2$   $t$ , we then choose a value of  $z$ . We choose a

value, consistent with the infrared cutoff at the lowest mass (the one used to compute  $\gamma$ ), according to the Altarelli-Parisi splitting function  $P(z)$ . If the chosen value of  $z$  is outside the allowed range at the actually chosen value of  $t$ , one chooses a new  $t$  and  $z$ , starting with the previously chosen  $t$  as the maximum value. This is how we allow for the mass dependence of the infrared cutoff.

Once  $t$  and  $z$  have been chosen, we can choose the azimuthal angles and spin of the gluons by the following procedure. When a quark emits a gluon, the azimuthal angle is chosen uniformly. The density matrix of the gluon is computed and stored. When an internal gluon decays into two gluons, one first contracts the density matrix with the (already computed) density matrix of the decaying gluon. The azimuthal angle is chosen according to the trace of this over the spins of both daughter gluons. The density matrix for each gluon is this traced over the other child's spin. When an internal gluon decays into a  $q\bar{q}$  pair, one chooses the azimuthal angle according density matrix, contracted with the (already computed) gluon density matrix.

Because the emission of a gluon off a gluon changes the spin of the gluon it is not practical to give closed formulae for the possible azimuthal dependences; the azimuthal dependence for a particular decay can depend on many branches of the tree. The emission of a low  $z$  gluon does not change the spin; in the  $z \rightarrow 0$  limit the density matrix of Eq. (2.9c) is dominated by the term whose spin structure is  $\delta^{ik} \delta^{i'k'}$ , that is, the term that gives the other child gluon the same spin as the parent. This means that any unresolved radiation does not affect the azimuthal angle.

If there are quarks in the initial state, the kinematics are changed; this is described in detail in chapter 4.

The discussion above holds, for the most part, for massive quarks. The infrared cutoff, requiring  $z$  such that the partons are on shell depends on the current mass. This effect is important only for gluons decaying into massive pairs. That, in turn, is important only for observables that detect the presence of heavy quarks. The other effect is that a massive quark radiates less than a massless quark with the same (off shell) mass. The function  $\Pi$ , expressing the probability of going between two off shell masses is given by<sup>5</sup> :

$$\Pi(t_{\max}, t) = \left( \frac{\log(((\sqrt{t} + m)^2 - m^2) / \Lambda^2)}{\log((t_{\max} - m^2) / \Lambda^2)} \right)^{\gamma/b}, \quad (2.20)$$

where  $m$  is the current mass of the quark.

We have seen how to compute the leading log approximation to the cross-sections for producing multi-parton final states correctly, and how to incorporate the results into a shower Monte Carlo program. It is possible to incorporate more accurate computations of the parton cross sections into the leading log approximation based shower program. There is some reason to believe that it is important to do so. In  $e^+e^-$  annihilation the exact order  $\alpha_s^2$  calculation for many observables differs from leading log approximation calculations by 30% or more<sup>6</sup>. One approach to incorporating the exact result into the shower Monte Carlo is to generate the events by the leading log approximation and to give them weights by the exact result (for the first four partons). Another approach which is possible for the simple case of  $e^+e^-$  is to generate two and three parton events according to the order  $\alpha_s^2$  cross section, generating 4 parton events in some fashion, weighted by the cross section. Multiparton events can be generated by allowing the four parton systems to radiate according to the leading log approximation.

## References for Chapter 2

- [1] For example,  
P. Mazzanti and R. Odorico, *Phys. Lett.* **95B** (1980) 133; *Z. Phys.* **C7** (1980) 61.  
R. D. Field and S. Wolfram, *Nucl. Phys.* **B213** (1983) 85;  
T. D. Gottschalk, *Nucl. Phys.* **B238** (1984) 349.
- [2] R. Odorico, *Nucl. Phys.* **B172** (1980) 157.
- [3] G. C. Fox, Proc. 1981 SLAC Summer School (1981), ed. A. Mosher.
- [4] G. Altarelli and G. Parisi, *Nucl. Phys.* **B126**(1977)
- [5] T. D. Gottschalk, *Nucl. Phys.* **B227** (1983) 413.
- [6] W. Bartel, *et al.*, *Phys. Lett.* **119B** (1982) 239.

### 3. Hadronization Models

#### 3.1. Independent fragmentation—the Field Feynman model

We now turn to models for forming hadrons out of a collection of partons generated by a leading log or other perturbative QCD calculation<sup>1</sup>. This process is called hadronization. The oldest model is the so-called Field-Feynman model<sup>2</sup> (FFM.) Two models in current use are those of Ali<sup>3</sup> and Hoyer<sup>4</sup>. The basic process of the FFM is the radiation of a meson by a quark. For instance, a  $u$  quark might radiate a  $\pi^+$  leaving a  $d$  quark of lower energy. The energy of the meson is distributed according to a function, called the fragmentation function:

$$\frac{dP}{dz} = f(z, Q^2) \quad (3.1)$$

where  $z$  is the ratio of the hadron's energy to that of the quark and  $Q^2$  is an energy scale in the problem. The dependence of  $f$  on  $Q^2$  can be calculated perturbatively<sup>5</sup>; the  $z$  dependence cannot. There is, in principle, an independent distribution function for each type of quark and meson. The direction of the hadron's momentum is chosen, in order to agree with experiment, to produce jets of limited transverse momentum; that is, so that the momentum of each of the radiated hadrons is, more or less, along the direction of the quark's momentum. Each meson is given a momentum transverse to the quark,  $p_t$  distributed according to:

$$\frac{dP}{d^2p_t} \propto e^{-p_t^2/2\sigma^2}. \quad (3.2)$$

The mesons are assumed to be vector mesons or pseudoscalars; the ratio between the two spins is an input parameter. The process of radiating a meson can be viewed as arising from the creation of a quark antiquark pair; the original

quark combines with the new antiquark to make the meson, leaving the newly created quark behind. The ratio of  $s\bar{s}$  pairs produced to  $u\bar{u}$  and  $d\bar{d}$  pairs produced is also an input parameter.

If one wishes to hadronize a system of quarks and antiquarks, one begins with any of the partons, and lets it radiate a meson, according to Eqs. 3.1 and 3.2. The new parton resulting is likewise allowed to radiate a meson. This continues until the energy of the remaining parton falls below some cutoff. The other partons are treated in the same way. Finally, the soft partons remaining are combined into mesons.

Gluons are treated as quark antiquark pairs of random flavor. There is no theoretical reason for this, but it seems to work fairly well for  $e^+e^-$  annihilation. The momentum of the gluon is split between the quark and the antiquark according to some *ad hoc* distribution; there are different ones currently in popular use<sup>3,4</sup>. The model can also be extended to allow for baryon production; the basic baryon producing process is a quark creating two pairs out of the vacuum, which combine to form a baryon with two antiquarks left over.

The FFM can be tuned to agree well with the data<sup>6</sup>, although some of the parameters seem to be energy dependent. An event generator based on the FFM can be used to analyze a detector, or to study the effects of hadronization on some observable, for example, how the energy flow of the hadrons differs from that of the partons. The FFM as described, however, has, as was first realized by its proposers<sup>2</sup>, severe theoretical difficulties that prevent it from being used as a model for understanding the soft physics. Most of these problems are the result of hadronizing each parton independently. In the first place, the basic process involves a massless quark radiating massive mesons; this means that energy and momentum cannot be conserved simultaneously. One cannot

correct this by holding the quark sufficiently far off shell, as this would mean that the quark would be off shell by the mass of the jet, which is generally large enough so that one should expect to be able to describe things perturbatively. A related difficulty is that the cutoff procedure cannot be made frame independent; this means, for example, that a Lorentz boost can change the mean number of particles that a given quark produces. There are also several arbitrary parameters and several arbitrary functions.

Another severe problem is that the hadrons are produced in the wrong order. There are very general theoretical arguments that suggest that the hadrons with the most energy are produced last<sup>7</sup>; this receives some experimental support from experiments with heavy nuclei as targets<sup>8</sup>. In the FFM, however, the hadrons with the most energy are produced first; they must be produced before their parent quarks have radiated too much energy. Perhaps the most serious problem, though, comes from the assumption that the partons hadronize independently. A quark and a collinear gluon cannot be distinguished from a quark, much as an electron cannot, in the limit of zero mass, be distinguished from an electron and a collinear photon. This means one must consider a quark with a gluon collinear to it, within some finite resolvability criterion, as a single quark. The hadronization of a partonic system will not be continuous as a gluon moves across this cut.

### **3.2. String models—the Lund model**

We are thus led to consider models of hadronization in which the partons do not hadronize independently. Such models tend to be based on a QCD motivated picture of confinement, the string picture. In this picture, when one tries to separate a quark from an antiquark there are field lines between them,

analogous to the field lines between electric charges as one tries to separate them. The QCD field lines are confined to a tube of fixed width between the quarks<sup>9</sup>, which means that the field energy increases linearly as the quarks separate. At some distance it becomes energetically favorable to create a pair of quarks, splitting the flux tube. The energy required to produce the mass of the new quarks comes from the energy of the part of the flux tube no longer needed to connect the original quarks.

One model based on this picture is the Lund model<sup>10</sup>. The simplest case is  $e^+e^- \rightarrow q\bar{q} \rightarrow \text{hadrons}$ . One imagines a flux tube, sometimes called a string, stretched between the quarks. If the system were classical and pair creation impossible, the quarks would separate at the speed of light losing energy to the flux tube until they were at rest. They would then move closer, gaining energy from the flux tube; if the system were classical it would continue to oscillate. In fact, the string is broken by the creation of quark antiquark pairs as it stretches. Because the string is the same along its length one expects a uniform probability for pair creation along its length:

$$dP = P dx dt, \quad (3.3)$$

for a 1+1 dimensional problem. The 4-momentum of a substring is the sum of the 4-momentum of the original quark and the energy contained in the flux tube between the original quark and the pair creation point. To extend this model to 3+1 dimensions, one must allow the produced pairs to have momentum transverse to the string, i. e., for the quarks to have equal and opposite transverse momentum. This means that the quarks created must have some non-zero energy; to conserve energy they must replace a finite length of the string. It is argued that this production over a finite distance is a quantum

mechanical tunneling phenomenon, and it is asserted on the basis of an analogy with the Schwinger model (QED in 1+1 dimensions) that the probability for producing a pair of quarks with mass  $m_q$  and transverse momentum  $p_t$  is:

$$dP = dp_t^2 e^{-\pi m_t^2 / \alpha}, \quad (3.4)$$

where  $m_t$  is the so-called transverse mass,

$$m_t^2 = m_q^2 + p_t^2, \quad (3.5)$$

and  $\alpha$  is the energy per unit length of string.

Before going on to discuss the treatment of gluons, we should notice that, if the uniform probability for locating the break (Eq. 3.3) were adhered to throughout, the final strings left over would not have the right masses to be mesons. One must force adjacent breaks of the string to be correlated to leave remnants with the mass of a meson with the quark content of the remnant. As in the FFM, it is assumed that the mesons are either vectors or pseudoscalar, with the ratio between these fixed by experiment.

The Lund model treats gluons by an extension of this string model. Consider, for example,  $e^+e^- \rightarrow q\bar{q}G \rightarrow \text{hadrons}$ . The gluon has the color quantum numbers of both a quark and an antiquark, and it has some momentum so it can be considered as a kink in the string connecting the quark and antiquark; that is, as connected to both ends of the string, but moving in some direction other than along the direction of the quarks. The gluon thus stretches the string more than it would be stretched by the quarks alone. This means that there will be more breaks than there would otherwise be. Some of the particles will get most of their momentum from that of the gluon; others, from one of the quarks. The result, if each of the partons has enough energy in the center of mass frame, is

a three-jet event, one jet along the direction of each of the partons. Events with more gluons hadronize as strings with more kinks.

In this picture, everything is quite smooth as a gluon becomes collinear with a quark. As that happens, the extra stretching of the string because of the gluon, compared to a system with two quarks, one of which has absorbed the momentum of the gluon, vanishes smoothly, so a system of partons in which a gluon is becoming collinear with a quark smoothly approaches the system with only a quark with the combined momentum. The other theoretical problems of the FFM are also corrected in the Lund model. The model is Lorentz invariant, the behavior being determined by the invariant masses of the strings, and it conserves energy and momentum naturally. The softer hadrons are produced first. While there are still several arbitrary parameters, the fragmentation functions are determined by the model's assumptions.

Like the FFM, the Lund model can be adjusted to agree well with experiment<sup>6</sup>. One should not, however, conclude that the Lund model and the FFM differ only in the semantics and approach; there are differences in their predictions. The most important differences between the models are direct consequences of the FFM's hadronizing partons independently and the Lund model's connecting partons by flux tubes. In a model with independent fragmentation, like the FFM, the jet from any parton is centered about the direction of its momentum. In a string model the string, which will eventually break into the hadrons, is being dragged along, in an event with gluons, by the kinks, that is, the gluons. The string based picture will predict that the particles of one jet are shifted toward the next gluon jet, whereas the independent fragmentation model will predict that one jet is independent of the others. Experiments at PETRA seem to confirm the string picture<sup>11</sup>.

The Lund model, however, also has some aspects that are theoretically troubling. These come from the constraint that the breaks in the string are correlated to produce hadrons of the correct mass. It is not easy to see how a quantum mechanical tunneling effect, in a semiclassical picture such as the string picture, can produce such constrained pairs. This makes the assumptions about the production of transverse momentum quite doubtful. In addition the rather cumbersome constraints required to implement these correlations make it difficult to see how a prediction of the model is related to its assumptions and parameters.

### 3.3. Cluster models

We are, then, led to consider a version of the string model that is free of the need for correlations between breaks of the strings. One way to assure this would be to break the string into segments each of which is in the multihadron continuum. An early model that used this idea of using the fundamental physics to derive the formation of bits of hadronic matter in the continuum was that of Hamer and Peierls<sup>12</sup>, which used multiperipheral Regge theory to describe the formation of clusters of hadronic matter that decayed according to the statistical bootstrap model to describe the width of the diffractive peak and central pion production in low  $p_t$  proton proton scattering. This model was used by Berger and Fox<sup>13</sup> to understand experimental data for multiparticle production at Fermilab and the ISR. The phenomenological success of the cluster approach and its theoretical advantages suggest the use of a model where the strings break into clusters of hadronic matter. Such a model is the QCD cluster model, which was developed by Gottschalk<sup>14</sup> incorporating ideas from the Lund model and from Field and Wolfram<sup>15</sup>. In this model, strings are put between the

perturbatively generated partons and broken, as in the Lund model. They are broken, however, not into individual mesons, but into color singlet subunits, called clusters, which have a mass of about one or two GeV. The decay of the clusters into hadrons is determined entirely by low energy experiment. This can be implemented by having the clusters decay into hadrons by a phase space model. Since the string breaking is into the continuum of multihadron states, there is no need to impose correlations between the breaks of the string. In addition, because momentum transverse to the direction of the string is generated by the phase space decay of the clusters, there is no need to assume the exponential fall off of  $p_t$  at the string breaks; the  $p_t$  distribution of a jet is a result of this model. A version of the cluster model is used in this thesis; this version is discussed in detail in Chapter 4.

The QCD Cluster model does not try to explain how the partons make up individual hadrons. The ideas about QCD dynamics incorporated into the model are used to describe the formation of the clusters. The formation of the hadrons from clusters is determined empirically from low energy experiments. The cluster decay model was determined as nearly as possible from low energy experiments where one can observe the decay of a single cluster. It is a basic assumption of the QCD cluster model that the hadronization of a cluster does not depend on the process that produced the cluster, only on its mass and quantum numbers. The model divides a process into three stages. There are the hard radiation and hard scattering process described by perturbative QCD, the moderate scales described by the string model picture of QCD confinement, and soft physics described by the empirical phase space model.

There are differences in the predictions of the Lund and cluster models. Both models allow production of baryons and strange particles at the string

breaks, by creating a pair of strange quarks or two quark antiquark pairs. The rate of production at this stage is an input parameter of both models. The QCD cluster models also allow production of strange particles and baryons in the phase space decay. The amount of production here will depend on the mass distribution of the produced clusters, thus, on the energy scale of the problem. Thus, if one considers the process  $e^+e^- \rightarrow q\bar{q} \rightarrow \text{hadrons}$ , the ratio of, for example, protons to pions is energy independent in the Lund model, but energy dependent in the cluster model.

There are similar results for the transverse momentum of a jet. In the Lund model there are two sources of transverse momentum. One is from hard QCD radiation. This dominates events with large transverse momentum relative to, say, the original quark directions. These events have high transverse momentum because one of the original quarks gives rise to two jets, one along the direction of the gluon, and one along the direction of the remnant quark. The other source of transverse momentum governs the distribution of hadrons within a jet; here the transverse momentum is generated at the string break, in the Lund model, according to Eqs. 3.4 and 3.5. These give a fixed transverse momentum distribution for a jet, independent of its energy. In the cluster model, on the other hand, the transverse momentum distribution of a jet is determined by the distribution of cluster masses. This model predicts a slight broadening of a jet as its mass increases. This is observed experimentally<sup>16</sup>.

### References for Chapter 3

- [1] A recent review is T. D. Gottschalk, CERN Preprint TH.3810-CERN, Lectures given at the 19<sup>th</sup> Int. School of Elem. Particle Phys., Kupari-Dubrovnik, Yugoslavia, (1983).
- [2] R.D Field and R. P. Feynman, *Phys. Rev. D* **15** (1977) 2590, and *Nucl. Phys. B* **139** (1978) 1.
- [3] A. Ali, E. Pietararian, G. Kramer and J. Willrodt, *Phys. Lett.* **93B** (1980) 155, and A. Ali, E. Pietararian and J. Willrodt, DESY Report T-01 (1980).
- [4] P. Hoyer, *et al.*, *Nucl. Phys. B* **161** (1979) 349.
- [5] R. D. Field, Lectures presented at the La Jolla Institute, 1978.
- [6] H. Obelack, Max Plank Institute preprint MPI-PAE/Exp.E1.110, Invited talk given at the 2<sup>nd</sup> Int. Confernece on Physics in collisions, Stockholm, June 1982.
- [7] J. D. Bjorken, Fermilab preprint FERMILAB-CONF-82/42-THY, Invited talk given at the 2<sup>nd</sup> Int. Confernece on Physics in collisions, Stockholm, June 1982.
- [8] C. Bromberg, *et al.*, *Nucl. Phys. B* **171** (1980) 38, K. Yung, Caltech Ph.D. Thesis, 1979.
- [9] R. P. Feynman, Lecture presented at 1981 EPS Int. Conf. on High Energy Physics, Lisbon, Portugal, Jul. 9-15, 1981.  
A. Casher, J. Kogut and L. Susskind, *Phys. Rev. Lett.* **31** (1973) 792.
- [10] B. Andersson, *et al.*, *Phys. Rep.* **97** (1983), 31 and references therein.

- [11] W. Bartel, *et al.*, DESY preprints DESY-83-079, DESY-83-080 (1983).
- [12] C. J. Hamer and R. F. Peierls, *Phys. Rev. D* **8** (1973) 1358.
- [13] E. L. Berger and G. C. Fox, *Phys. Lett.* **47B** (1973) 162.
- [14] T. D. Gottschalk, *Nucl. Phys.* **B214**, (1983) 201,  
T. D. Gottschalk, *Nucl. Phys.* **B238** (1984) 349.
- [15] R. D. Field and S. Wolfram, *Nucl. Phys.* **B213** (1983) 85;
- [16] P. Soding and G. Wolf, *Ann. Rev. Nucl. Sci.*, **31** (1981) 231.

## 4. Event Generation in Hadron Hadron Scattering

### 4.1. Introduction and overview

We now present in detail the methods and algorithms used in an event generator for hadron hadron scattering. There are several steps involved. We shall first list the steps to give an overall picture of the model, and then return to describe each step in detail.

- 1: A parton that will evolve into the parton which will undergo the hard scatter is selected from each of the hadrons. Its type, energy, and momentum are chosen according to some empirically determined wavefunction that describes the partons in the hadrons at some low mass scale.
- 2: These partons are allowed to evolve, by radiating partons, to a scale  $Q^2$ ; i. e. the partons are allowed to radiate partons with timelike 4-momenta making their 4-momenta more spacelike, so long as  $p_\mu p^\mu \geq -Q^2$ , at which point the parton has evolved the right amount to undergo the hard scatter.  $Q^2$  is integrated over at the end. At this stage we have computed the scale dependent distribution function at the appropriate scale, and found a collection of partons resulting from the evolution of the distribution, which will later hadronize.
- 3: These partons then undergo a hard  $2 \rightarrow 2$  scattering, generating two new partons with timelike 4- momentum; each of these partons has a momentum  $k_i$  transverse to the direction of the scattering partons, in their center of mass frame, of magnitude  $|k_i^2| = Q^2/4$ .

- 4: The resulting system of partons evolves by radiation of partons to a cutoff scale; that is, until the off shell mass of the partons is less than some specified value. Fig. 4.1 shows a schematic picture of the model at this stage.

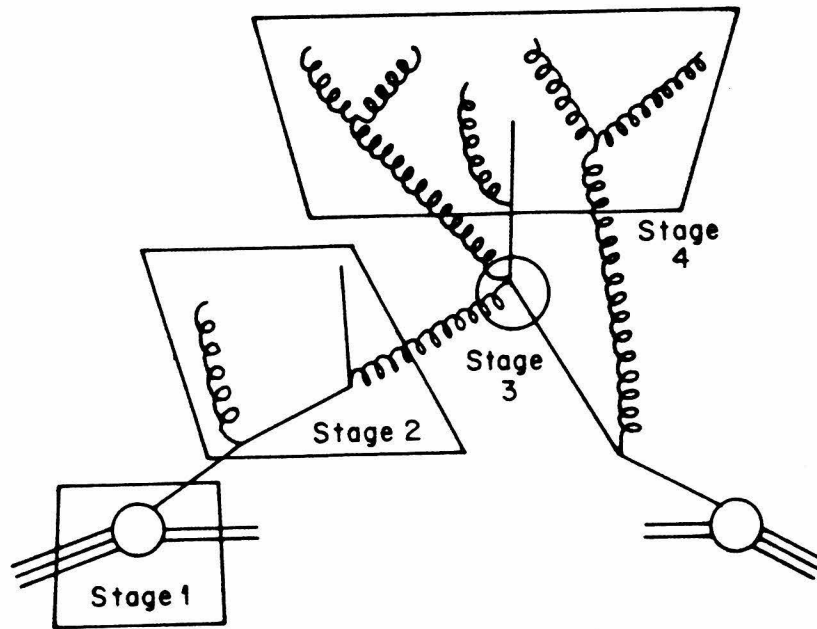


Fig. 4.1

A diagrammatic representation of a hadron-hadron event at the parton level. The lower events are the stages described first above. The hard scatter is circled.

- 5: Color singlet subunits of the event are formed from the generated partons. These will be hadronized according to the cluster model.
- 6: The spectator partons, the parts of the hadrons not involved in the hard scatter, are now included. They give rise to the beam jets in the ensemble of partons.

- 7: The resulting system of "final state partons" is then hadronized according to a version of the QCD cluster model.

#### 4.2. Choosing the initial partons

The wavefunctions that govern the selection of the initial partons (step 1.) called distribution functions, are determined in deep inelastic lepton scattering. In this process, a lepton is scattered against a hadronic target. The scattered lepton's 4-momentum is measured; the hadronic final state is not. The momentum of the quark off which the lepton scattered can be determined by the scattered lepton's 4-momentum. In the infinite momentum limit:

$$p^\mu = xP^\mu, \tag{4.1}$$

where  $p$  is the parton momentum,  $P$  is the hadron's momentum, and  $x$  is given by

$$x = \frac{Q^2}{(2P \cdot q)}, \tag{4.2}$$

where  $q$  is the 4-momentum transfer and  $Q^2$  is  $-q^2$ . By choosing different leptons ( $\mu$ ,  $\nu$  and  $\bar{\nu}$ ) and different hadrons ( $p$  and  $n$ ) one can measure all the quark distributions, as functions of  $x$ . Since the gluons do not couple directly to any currents that the leptons do, the gluon distribution function cannot be determined directly from deep inelastic scattering data. Some information about the gluon distribution can be inferred from the fact that whatever momentum of the hadron is not carried by the quarks must be carried by gluons.

The distributions will depend on the scale  $Q^2$  at which the experiment is performed. This scale dependence arises because the partons can radiate more gluons or produce more quark pairs as they evolve to a higher scale than they

can at a lower scale. The gluon distribution function at one scale contributes to the quark distribution function at a higher scale because the gluons produce quark pairs. One can, using this fact, make some inference about the gluon distribution at low scales. The distribution function for the sea quarks, that is the pairs in addition to the valence quarks which determine the hadron's type, depends strongly on the gluon distribution. One can measure the sea distribution by, for example, looking for signals from  $\bar{c}$  quarks produced off  $\bar{s}$  and  $\bar{d}$  quarks in antineutrino nucleon scattering.

The partons can also have momentum transverse to that of the hadrons; this can be measured, for example, in the production of  $\mu$  pairs in hadron hadron scattering. The muons are produced by processes like  $q\bar{q} \rightarrow \gamma^* \rightarrow \mu^+\mu^-$  and  $qG \rightarrow q\gamma^* \rightarrow q\mu^+\mu^-$ .  $\mu$  pairs with invariant mass  $Q^2$  give information about partons at a scale of  $Q^2$ ; from the transverse momentum distribution of the pairs (that is, the momentum of the pair transverse to the collision axis) one can infer the transverse momentum distribution of the partons.

For the hadron hadron event generator we use the distribution functions at some fixed, small scale. The evolution to the variable scale  $Q^2$  is governed by perturbative QCD and is calculated during the event generation process. This procedure is suggested by the success of the scale dependent distribution functions in describing deep inelastic scattering cross sections, where it is theoretically sound<sup>1</sup>. When one considers the hadronic final state, however, this approach is open to question on theoretical grounds. In particular it leads to difficulties with the beam remnants; a detailed discussion of this is deferred until we reach the discussion of the beam remnants (step 6.)

For the analysis of chapter five we have chosen the following distribution functions for the proton. There are valence distributions for the  $u$  and  $d$

quarks, an SU(3) symmetric sea, and a gluon distribution.

$$u_v = 5.94 \frac{(1-x)^3}{x^3} - 2.88 \frac{(1-x)^3}{x^{15}}, \quad (4.3a)$$

$$d_v = 2.88 \frac{(1-x)^3}{x^{15}}, \quad (4.3b)$$

$$Sea = .202 \frac{(1-x)^{10}}{x}, \quad (4.3c)$$

for each species, and

$$G = 2.64 \frac{(1-x)^5}{x}, \quad (4.3d)$$

or

$$G = 6.05 \frac{(1-x)^{10}}{x}. \quad (4.3e)$$

The transverse momentum distribution at  $Q^2 = 1.8$  GeV was taken to be Gaussian, with mean transverse momentum of 700 MeV.

The distribution functions are based on those of Buras and Gaemers<sup>2</sup>, which are extracted from deep inelastic scattering data. They differ from those of Buras and Gaemers only in that the exponents of  $(1-x)$  in the valence distributions were rounded to the nearest integer, 3, for computational convenience. The difference is significant (more than about 10%) only for values of  $x$  so large ( $\gtrsim .7$ ) that both distributions are quite small and the discrepancy does not have much effect on the result. Any charm component of the proton, at that scale, has been neglected. The transverse momentum is chosen to be comparable to Ref. 3. It is chosen to be independent of the flavor of the parton for

convenience; there is no experimental evidence compelling any other choice.

These distributions have non-integrable singularities as  $x \rightarrow 0$ ; that is, there are an infinite number of partons in a proton. The integral of  $x$  times the sum of the distribution functions is 1, which is just the statement that the partons carry all the momentum of the proton. To choose an initial parton from the proton we put some lower limit on the energy of the parton that will eventually undergo the hard scatter. This can be done without affecting the result, as the two active partons, with spacelike momentum, must have at least enough energy to wind up with the correct transverse momentum. The cutoff used is:

$$E_c = \frac{Q}{\alpha - Q/E_{cm}}, \quad \alpha = 4, \quad (4.4)$$

which was determined empirically by raising  $\alpha$  until the cross section calculated no longer changed. The exact form of the cutoff is not important; what is important is that the cutoff be greater than 0 and that no parton with energy less than the cutoff has a chance of finding a partner with which to undergo the hard scatter. To make the program efficient, the cutoff should be as high as possible. The form of the cutoff, a fraction of  $Q$ , with the fraction required rising as a  $Q$  does, comes from the following picture. The two (spacelike) partons are approaching each other more or less head on, in the event center of mass frame; each one has a momentum larger than its energy. The momenta largely cancel, leaving a system with timelike momentum. To become a real event at any  $Q^2$  the system must have a mass of at least  $Q$ ; in the typical event the two incoming SLPs have comparable energies and momenta, but some imbalance does occur; hence the cutoff is a fraction of  $Q$ . As the partons get more off shell and the required energies get larger the relative imbalance permissible decreases; hence the cutoff gets closer to  $Q/2$ . Empirically, partons with

energies below the cutoff of Eq. 4.4 do not find other partons with which they can combine to make a hard scattering event. Once the cutoff is determined, one can choose a parton type, each type having the probability:

$$P_i = \int_{\xi}^1 f_i(x) dx / \sum_j \int_{\xi}^1 f_j(x) dx, \quad (4.5)$$

where  $f_i(x)$  is the distribution function for parton type  $i$ ,  $\xi$  is the cutoff, and the sum is over all parton types. Once the type is chosen the value of  $x$  is chosen according to:

$$\frac{dp}{dx} = \frac{f(x)}{\int_{\xi}^1 f(x) dx}. \quad (4.6)$$

The transverse momentum of the parton is then chosen according to the Gaussian distribution. For the moment the transverse momentum is chosen along the  $y$ -axis, the  $z$ -axis being the beam axis; the collection of partons will later be rotated by a random angle in the  $xy$ -plane before being combined with another set to make the hard scattering event. The parton is given a weight

$$W = \sum_j \int_{\xi}^1 f_j(x) dx, \quad (4.7)$$

which will be used later to compute the contribution to the cross section of an event involving this parton.

### 4.3. The evolution to the scale $Q^2$

In step 2 the parton is allowed to evolve, according to the formalism in chapter 2, to the previously chosen scale  $Q^2$ , see Fig. 4.2. Because we are, in this phase, considering a parton with spacelike momentum evolving towards more spacelike momentum, the kinematics is slightly different from the description in chapter 2. We now have a parton with spacelike momentum radiating a parton

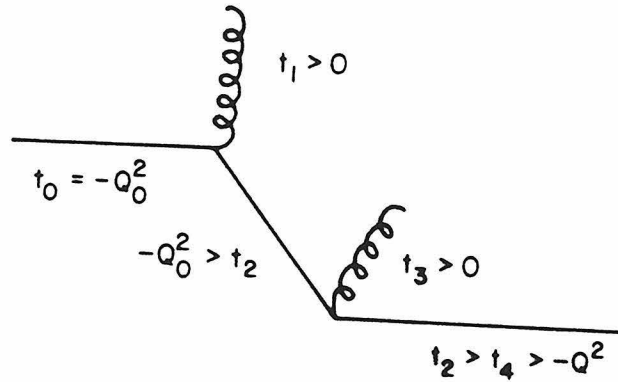


Fig. 4.2

A parton comes from the hadron (on the left) and evolves to the hard scatter (on the right).

with timelike momentum, leaving a parton with spacelike momentum with a more negative  $mass^2$ . The momentum distributions for each vertex are determined by the formulae of chapter 2, with  $t$  everywhere replaced by  $|t| = -t$ . If one were to compute the density matrices by the procedures used in chapter 2, noting that the nonnegligible mass was that of the daughter with a spacelike momentum, one would find that each density matrix differed from the result of chapter 2 by an overall factor of  $-1/z$ . The minus sign is what changes  $t$  to  $-t$  in the denominators, and the factor of  $1/z$  can be absorbed in converting the flux factor in the cross section from that for the hadrons to that for the partons. We shall do so here, using parton  $2 \rightarrow 2$  cross sections rather than matrix elements squared in computing the event cross section. The choice of  $-t$  for the argument of  $\alpha_s$  is arbitrary and taken for convenience only; any change in the coefficient of  $t$  in the argument of  $\alpha_s$  is a subleading correction.

To implement the procedures described in chapter 2, one needs some sort of cutoff to avoid the singularity as the four momentum of a gluon goes to zero. We cannot use the same cutoff here that was described in chapter 2 and used for

the decay of a parton with timelike momentum; i. e., that the value of  $z$  should be such that both daughter partons could be on shell, since this is not kinematically possible. A variety of resolvability cuts can be imagined: cuts on the energy of the particles, their transverse momentum, a cut at fixed  $z$  and so on. There is no firm theoretical basis for choosing one particular cut. Earlier work by Fox<sup>4</sup> has suggested that the exact nature of the cutoff used is not crucial. We, for calculational convenience, use an energy cut, typically 1 GeV. This was checked empirically by lowering the value and seeing that neither parton level cross sections,  $d\sigma/dk_t^2$  nor variables describing the shapes (energy flow) of the full events were significantly changed. With this value of the cutoff, the disallowed radiations would almost always have less than 300 MeV of momentum transverse to that of the parent, so it is a reasonable value for a resolvability cut. The cross sections are much more sensitive to the value of the cutoff below a region around 1 GeV, as the partons radiate too much as the cutoff get too close to the singularity. Observables that describe the energy flow of the events are changed if the cutoff is raised too much above 1 GeV; this is a sign that, with such a high cutoff, radiation that should be considered resolvable is being treated as irresolvable.

The issue of the resolvability cut is quite problematic. To say that a particular radiated gluon is not resolvable is to say that it does not significantly affect anything, once the strong interactions have gathered everything into hadrons; that is, that the strong interaction spreads its energy and momentum among hadrons in such a way that there is no real remnant of the radiated particle. Thus, in the string picture in spacetime, the resolvability criterion is that a radiated gluon travel a distance transverse to the string comparable to the string's width before being brought to a stop by the strong forces. It is not clear how to

implement this; neither the string formation, nor the forces that would slow a parton moving across the string are well enough understood. It would seem though, that a transverse momentum cut of some sort is more likely than the energy in the event center of mass to be, conceptually, the best choice. It is not, however, clear what transverse momentum cut to implement. There are several sensible sounding choices: relative to the parent, relative to the beam direction, or relative to some other estimate of the string's direction. In addition, the value of the cutoff might depend on the longitudinal momentum. It is not clear which of these would be best, and all are harder to implement than the energy cut. Relying on the work of Fox, which showed that whether the cutoff for resolvable radiation for the partons with timelike momentum was a cutoff on the parent mass (as is now used), on the energy, or the transverse momentum did not matter much, we chose an energy cut for convenience.

The procedure for determining a radiation is as follows. It is determined whether the parton will radiate, and if so to what value of  $|t|$ . This is determined according to the procedure in chapter 2, with  $\Pi$  given by:

$$\Pi(t_{\max}, t_{\min}) = \left( \frac{\log(-t_{\max}/\Lambda^2)}{\log(-t_{\min}/\Lambda^2)} \right)^{\gamma/b}, \quad (4.8)$$

where both  $t_{\max}$  and  $t_{\min}$  are less than 0. Here the value of  $t$  chosen is not that of the parent, but of the daughter with spacelike momentum. The value of  $z$ , the energy fraction carried by one of the daughters, is chosen according to the Altarelli-Parisi splitting function. The energies of the two daughter partons are computed. If both are below the cutoff of Eq. 4.4, the event is rejected; the number of rejected events is stored for use in computing the cross section. The fraction of events accepted is the Monte Carlo estimate of the fraction of the partons with  $z$  above the cutoff at the scale  $Q_0^2$  that still have  $z$  above the cutoff

after evolving to the scale  $Q^2$ , that is:

$$\frac{\int_{\xi}^1 f(x, Q^2) dx}{\int_{\xi}^1 f(x, Q_0^2) dx}, \quad (4.9)$$

where  $\xi$  is the cutoff and  $Q_0$  is the scale at which the wavefunctions are taken. If only one of the energies is above the cutoff of Eq. 4.4, that parton is chosen as the parton with spacelike momentum and the process continues. If both partons have enough energy then one is chosen at random to be the parton with spacelike momentum. The weight of the event is multiplied by two, in this case, to compensate for the  $1/2$  chance that each parton was chosen, since the correct weight for each choice is 1.

This process is repeated until it is determined that the parton with spacelike momentum does not radiate further below the scale  $Q^2$ . Decay chains are not computed for the parton with timelike momentum generated at each vertex until it is known whether a usable event will be generated. Only the mass at which the parton with timelike momentum decays, which is needed to compute the kinematics of the radiation, is computed at this stage. At this point the computed decay chain is stored and the process is repeated until there is a collection of events each with a parton with spacelike momentum that has been evolved to the scale  $Q^2$ . The energy distributions of these partons of different type are the  $f_i(x, Q^2)$ .

There is no sure theoretical guide to choosing the scale  $Q^2$  to which the partons are evolved. We can tell only that it should be some scale determined by the kinematics of the parton level hard scatter. Since we are evolving the partons, rather than using some parameterization of the  $Q^2$  dependent distribution functions, we must, if the final program is to be efficient, choose some definition that depends neither on the result of the evolution, for instance on the value of

$x$  for the final active parton, nor on the other parton in the hard scatter. An example of a choice of  $Q^2$  that must be rejected on this basis is the invariant  $mass^2$  of the two partons undergoing the hard scatter. If we chose that as our definition of  $Q^2$  we would not be able to determine how far to allow a quark to evolve before knowing what the momenta of the two final partons with spacelike momentum coming into the hard scatter were. The choice we have used is  $Q^2=4k_t^2$ . To calculate any observable, we calculate the observable by Monte Carlo simulation at fixed  $Q^2$  and then integrate over  $Q^2$  by a trapezoidal integration.

#### 4.4. Hard scatter and cross section

The third step is to compute the hard scatter. Two of the previously generated final partons with spacelike momentum are chosen at random. The second parton and the other partons associated with it are reflected through the plane normal to the beam axis and rotated by a random angle about the beam axis. (If an observable without azimuthal symmetry is considered, the final event must also be rotated by a random angle about the beam axis.) If the collision considered is  $p\bar{p}$ , the partons associated with the second parton are replaced by their charge conjugates. The two final partons with spacelike momentum are combined; if the invariant mass of the two is high enough to allow a scatter with the required  $k_t$ :

$$k_t^2 = Q^2/4 \tag{4.10}$$

the event is accepted; otherwise it's rejected. The numbers of accepted and rejected events are computed, for later use in determining the weights for the events. If the event is acceptable we determine which parton has the positive

$z$ -momentum and what types they are (if there's a choice) according to the cross sections for on shell partons. A table of the acceptable events is made and stored for later use.

When the desired number of acceptable events has been accumulated they are considered one at a time. The weight for any event is:

$$W = W_1 W_2 f_z^2 f_s \frac{d\sigma}{dk_t^2}, \quad (4.11)$$

where  $W_1$  and  $W_2$  are the weights associated with the two partons that have been combined,  $f_z$  is the fraction of of the attempts to evolve a parton to this  $Q^2$  that gave a final parton with spacelike momentum with enough energy (above the cutoff in Eq. 4.4),  $f_s$  is the fraction of the attempts to have two partons undergo a hard scatter where the two partons with spacelike momentum had a high enough invariant mass, and  $\frac{d\sigma}{dk_t^2}$  is the QCD cross section for the  $2 \rightarrow 2$  hard scatter (to order  $\alpha_s^2$ ).  $1-f_s f_z^2$  is the fraction of attempts at generating an event where either one of the partons with spacelike momentum evolves below the cutoff (Eq. 4.4) or the combination of the two partons with spacelike momentum, after evolving, has too low an invariant mass to undergo the hard scatter. Thus the factor  $W_1 W_2 f_z^2 f_s$  is the flux of suitable partons, in units of the hadronic flux. The decay chains are computed according to the leading log approximation, so when we are done we have parton level events distributed according to the cross sections in the approximations discussed above, that is, order  $\alpha_s^2$  for the hard scatter and the leading log approximation everywhere else. We assume that hadronization does not affect the cross section; every parton level event is hadronized with weight 1.

This last assumption cannot possibly be exactly true; one need only consider the  $e^+e^-$  annihilation cross section as the energy passes through a region

of resonances (like the  $\psi$  region) to see this. At high energies, it is reasonable to expect that the hadronization does not have much effect on the cross section since hadronization effects are asymptotically suppressed by powers of the energy scale relative to the leading effect. In  $e^+e^-$  annihilation to hadrons at high energy the cross section<sup>5</sup> is in agreement with parton level calculations within the experimental uncertainty, so there is experimental support for this assumption as well.

#### 4.5. Parton evolution after the hard scatter

In step 4 the partons with timelike momentum are allowed to evolve to a cutoff scale  $t_{cut}$  according to the leading log approximation developed in chapter 2. This includes the partons with timelike momentum generated at the hard scatter, as well as those generated as the partons with spacelike momentum evolve to the scale  $Q^2$ . For this part, the momentum fraction variable  $z$  is identified with the fraction of  $E+|\mathbf{p}|$  of the parent carried by one of the daughters, measured in the rest frame of the parent's parent<sup>6</sup>. With this choice, the leading log approximation gives correctly both the leading term and the first subleading term in the order  $\alpha_s$  cross section for  $e^+e^- \rightarrow q\bar{q}G$ . The cutoff to avoid the singularity as the 4 momentum of a gluon goes to zero is that  $z$  must be such that it would be consistent for both daughter partons to be on shell. The masses of those partons that do not radiate before  $t_{cut}$  are chosen at random between 0 and  $t_{cut}$ , consistent with the exact kinematics. This does make some difference, as is discussed in chapter 5.

#### 4.6. Formation of the clusters

Step 5 begins the hadronization process. The first stage in this process (step 5) is to organize the final partons into the initial color singlet clusters. Each gluon is split into a quark and an antiquark; the flavor is chosen at random, the relative probabilities for the different flavors is an input to the model. The momentum of the gluon is shared between the two quarks; the fraction carried is chosen uniformly. The predictions of the model are not sensitive to the distribution used for the momentum sharing, provided that it is symmetric between the quark and the antiquark. We now have a final system of quarks and antiquarks. If one starts with a color neutral string, one can track the string through its evolution in the leading log approximation since there is no interference. For example, consider the three parts of Fig. 4.3.

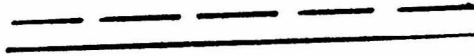


Fig. 4.3a

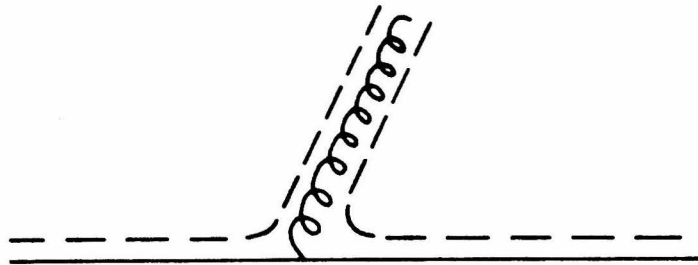


Fig. 4.3b

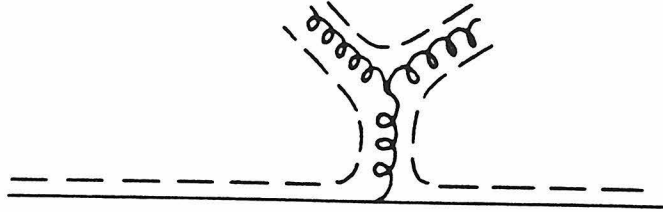


Fig. 4.3c

In the first diagram there is a quark; it is connected by a string to something with the color quantum number of an antiquark, a  $\bar{3}$ , which is not shown in the figure. When the quark radiates a gluon, which carries the color of the quark, 3, and a  $\bar{3}$ , the color 3 of the gluon is connected to the  $\bar{3}$  not shown. The color  $\bar{3}$  of the gluon is connected to the quark, as shown in the second part of the figure. If the gluon were to radiate another gluon, the result would be as shown in the third part of the figure; the strings that had been connected to the radiating gluon are now connected to the daughter gluons, one to each daughter gluon. The remaining strings of the daughters are connected together. The (effective) quark and antiquark at the ends of each string are combined to make the initial color singlet clusters.

This procedure of splitting the gluons is completely *ad hoc*; in fact, the study reported in chapter 5 shows this to be phenomenologically unacceptable. The original motive for its use was that one could directly extract the hadronization properties of quark-antiquark clusters from low energy experiment, where gluons are unimportant. Splitting the gluons has given good results in  $e^+e^-$  annihilation. Chapter 6 suggests a version of the cluster model that does not require gluon splitting.

It is impossible to track the color evolution through the hard scatter in this fashion. For many of the  $2 \rightarrow 2$  processes it is not unique. Since there is

interference in the cross sections used, it is not possible to assign a correct probability to each of the possible ways of connecting the strings. The connection of the strings is chosen at random, each possibility given equal weight. The results do not seem to be sensitive to this; other possibilities were tried and did not seem to make any difference. While in particular gauges the interference terms can be made small, allowing one to track the color flow, there does not seem to be much point in using this to assign probabilities since it seems to be phenomenologically unimportant.

#### **4.7. The beam remnants**

We have, then, a collection of strings, each of which connects an effective quark with an effective antiquark. The only strings not like this are those connecting the partons originally selected to the rest of the hadrons. These are treated (step 6) by the procedure, described below, by which these remnants are treated.

The dynamics of the beam remnants is problematic. If one takes the "active" parton from the hadron at some fixed scale,  $Q_0^2$ , about the same order as hadron masses, the beam remnant will also have a mass of order  $Q_0^2$ . The beam jets actually have a much higher mass. If one pictures an event in space-time, there are the two scattered quarks and the two beam remnants, all colored, beginning to separate. There are strong forces involved in the color screening. If, as is suggested by the success of this method in describing deep inelastic scattering, we extract the active partons at a fixed scale and then evolve it, one of the effects of these strong forces must be to drive the beam remnants off shell. For our simulation the beam remnants are taken off shell by exchanging a constant amount of momentum along the beam axis between them

(750 MeV for the results discussed in chapter 5). This gives beam remnants with an invariant mass-squared  $Q'^2 \propto P_{beam}$ . If one imagined a string between the two colored beam remnants, and assumed that it would stretch and break like any other string, it would stretch for an amount independent of the beam remnants' momentum, and give fragments with  $mass^2 \propto P_{beam}$ .

One or two soft hadrons are taken from each beam remnant to conserve flavor quantum numbers according to the scheme described below, leaving the quark (or pair) needed to be put on the end of the string(s) connecting to the beam remnant. These quarks are allowed to evolve, as any other quark, as described above.

The flavor of the soft hadron(s) and the leftover quark(s) is chosen by a procedure that depends on the flavor of the initial parton. If it is a valence quark, a quark antiquark pair is created; the quark combines with the two remnant valence quarks to form a baryon, the antiquark connects to the string; as shown in Fig. 4.4a.

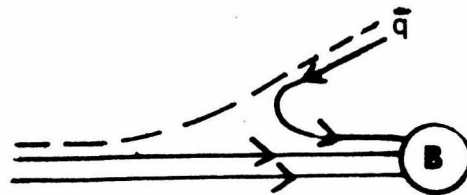


Fig. 4.4a

Beam remnants for an active valence quark. The two solid lines entering from the right are the remaining valence quarks; the dashed line is the string.

If the first parton is a gluon, two pairs are created. A quark and antiquark are chosen from these pairs, plus the valence quarks, to connect to the strings carried by the gluon. The remaining 5 quarks are combined, at random, to form a baryon and a pseudoscalar meson, as shown in Fig. 4.4b. If the initial parton was a quark other than a valence quark, a pair is created and added to the valence

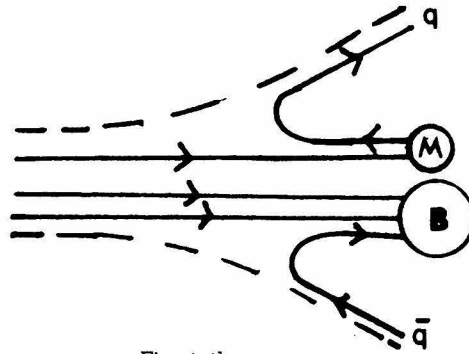


Fig. 4.4b

Beam remnants for an active gluon. The three solid lines entering on the left are the valence quarks. The two dashed lines are the strings.

quarks and the antiparticle of the selected quark. One (anti)quark is chosen at random to connect to the string; the remaining quarks are combined into a baryon and a pseudoscalar meson, as shown in Fig. 4.4c.

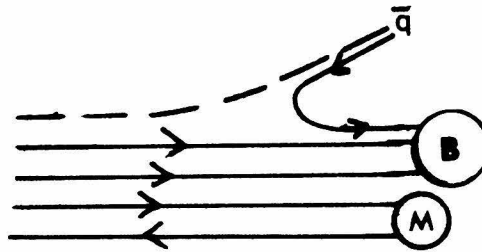


Fig. 4.4c

Beam remnants for an active nonvalence quark. The four solid lines entering on the left are the valence quarks and the antiquark of the nonvalence quark. The dashed line is the string.

The momentum of the hadrons is chosen by the following procedure. The baryon is given an energy fraction  $z$ , in the rest frame of the remnant, after it has been pushed off shell.  $z$  is distributed according to the probability distribution:

$$\frac{dP}{dz} = 2z, \quad (4.12)$$

which is chosen as a convenient way to get the baryon soft in the event's center of mass frame. Its momentum is taken opposite the direction that the remnant must be boosted to return to the event center of mass frame, so that it is soft in that frame. If there is a meson, its momentum and energy are determined in

the same fashion from the remaining mass. The leftover 4-momentum is given to the quark connected to the string, or split equally between the two quark connected to the strings in the case of an initial gluon. These quarks are allowed to evolve as described above.

There is no theoretical justification for the procedure used for the beam jet. It does satisfy certain requirements. It allows the beam jets to have enough particles, at least at ISR energies and lower. Because most of the particles are produced by the hadronization of the string, the beam remnant fragments like any other jet, in accord with experiment<sup>7</sup>. The colored beam remnant is able to radiate if its mass is high enough.

This rather clumsy procedure, involving extra baryons and so on, was required because, at the time the program was written, the string breaking model did not allow for strings with nonzero baryon number. It would now be possible to make (one of the) the string(s) connecting the remnant to the initial parton have baryon number. One would have to add a soft meson to conserve quantum numbers only if the initial parton were a nonvalence quark. The model of the beam remnant used here works well for describing energy flow at the energies studied in chapter 5; it does not work well at the energy of the SPS collider (540 GeV in the center of mass.) A modified version of this model, using baryonic strings would probably fare no better at high energy, so it does not seem worthwhile to implement. Some discussion of what can be done is in chapter 6.

#### 4.8. Hadronization

After the evolution of the beam remnant we are left with a handful of hadrons and some clusters, each with a quark and an antiquark. The last step, step 7, is to hadronize these clusters. The mass of each of the clusters is checked. If there is a cluster whose mass is less than a fixed cutoff (typically 250 MeV) above the two particle threshold for the flavors it contains, it is combined with another cluster, if possible, to get above this cut, by recombining a gluon that had been split into an effective quark antiquark pair. The gluon that had lesser mass, if two gluons were split to form the cluster, is chosen to be recombined. The momentum of the recombined gluon is shared between the two quarks making up the larger cluster. If there is no gluon involved the cluster is accepted. It is impossible to get a cluster below two particle threshold after the recombination, as the quark masses are chosen to be hadron masses; the  $u$  and  $d$  quarks are given the  $\pi$  mass; the  $s$  quark, the  $K$  mass, and so on.

The above procedure for combining clusters is purely arbitrary, and is done only so that every cluster will have some hadronic state of the right mass available into which to decay. The improved model suggested in chapter 6 will not give rise to such light clusters, which always come from splitting the gluons.

The final collection of clusters is hadronized according to the QCD cluster model, which is described in detail in Ref. 8. Here it will suffice to review some of the salient features. Clusters of a large mass (above some fixed cutoff) decay into other clusters by a 1+1 dimensional string model, as described in chapter 3. Breaks in the string occur with uniform probability per unit area of space-time swept out by the string, with the restriction that both daughter clusters have mass more than 250 MeV above two-body threshold. Lighter clusters decay by a phase space model. A cluster is allowed to decay into two-body states

**References for Chapter 4**

- [1] G. Altarelli and G. Parisi, *Nuc. Phys.* B126(1977)
- [2] A. J. Buras and K. J. F. Gaemers, *Nucl. Phys.* B132 (1978) 249.
- [3] R. D. Field and G. C. Fox, Invited talk presented at the Europhysics Study Conference on Jet Dynamics in Quark and Lepton Interactions, Erice, Sicily, Sep. 1982.
- [4] G. C. Fox, private communication.
- [5] E. Hilger, Invited talk given at 5<sup>th</sup> International Conference, "Novel Results in Particle Physics," Vanderbilt Univ., Nashville, Tennessee, May 24-26, 1982.
- [6] G. C. Fox, Proc. 1981 SLAC Summer School (1981), ed. A. Mosher.
- [7] C. Bromberg, *et al.*, *Phys. Rev. Lett.* 45 (1980) 769.
- [8] T. D. Gottschalk, *Nucl. Phys.* B238 (1984) 349.
- [9] T. D. Gottschalk, *Nucl. Phys.* B238 (1984) 325.

## 5. Comparison of the Model with Experiment

In this chapter we use an event generator implementing the model described above to study proton proton collisions producing high  $E_t$  final states. Hadronic reactions producing particles at large  $p_t$  or  $E_t$  are believed to be the reflection of hard scattering of a single parton from each hadron. In the most naive picture, such an event consists of four jets: the jets coming from the partons undergoing the hard scatter, and two jets along the beam axis coming from the remnants of the two hadrons. Early experiments studying this phenomenon concentrated on looking at single particle inclusive cross sections<sup>1</sup>. While they did find large cross sections for high  $p_t$  particles, they failed to observe the  $p_t$  dependence expected from the naive model. It was realized that these single particle cross sections are very sensitive to the fragmentation of the partons into jets and the transverse momentum of the partons in the original hadrons<sup>2</sup>. Later experiments attempted to find jets directly, using calorimetric measurements. The first experiments used calorimeters about the expected size of a jet<sup>3</sup>. The small size of the calorimeter made it difficult to determine whether the observed events were indeed jets or just the result of statistical fluctuations in nonjetlike events. Several experiments have been done using calorimeters much larger than the size of jets. We shall discuss results of the NA5 experiment<sup>4</sup>, E-557<sup>5</sup> and the AFS collaboration<sup>6</sup>. At lower energies  $\sqrt{s} \lesssim 30$  GeV the events are not jetlike. At higher energy the high  $E_t$  events are jetlike.

For this analysis a Monte Carlo simulation using the QCD Cluster model, described above, has been written, and compared with the experimental results. No parameters were tuned for this analysis. The agreement with experiment is generally good. Some disagreement is found; this points the way for improvements to the model, which are being worked on.

The model parameters, in addition to the hadronization parameters which were determined from  $e^+e^-$  annihilation, are  $\Lambda$ , the quark masses, the scale at which the perturbative evolution stops, and the distribution functions for finding the partons in the protons at some scale.  $\Lambda^2$  was fixed at  $.2\text{GeV}^2$ , the masses of the  $u$  and  $d$  quarks at 200 MeV, the  $s$  quark at 500 MeV, the  $c$  at 2 GeV and the  $b$  at 5 GeV. The top quark was presumed to be too heavy to be produced. The quark distribution functions were described in chapter 4. The dependence of various quantities on the cutoffs was checked. The cross sections depended moderately on the energy cutoff for the evolution before the hard scatter, the shape variables not at all, as the cutoff was varied from .5 to 1.25 GeV (the minimum energy of the gluon in the center of mass). This indicates that the model is insensitive to assumptions about the soft gluons generated at this point. (Since most of the energy is just motion along the direction of the emitting parton, these are soft.) None of the observables checked at NA5 depended noticeably on the cutoff for the evolution after the scatter. At higher energy the shape did depend on the cutoff for the evolution after the hard scatter. This matter is discussed below.

The program was used to simulate  $pp$  collisions at center of mass energies of: 23.8 GeV (NA5), 27.8 GeV (E-557), 30 GeV and 63 GeV (AFS). Between 30,000 and 60,000 events were used at each energy. The lower limit of the  $k_t$  integration was, in each case, 2 GeV. The upper limit varied with energy; it was large enough so that the cross sections for the  $E_t$  values shown in the figures were not significantly altered by the last  $k_t$  value. Events with  $k_t$  less than 2 GeV were not included, as there is little reason to expect perturbative QCD to describe the interactions of partons at such low energies. This means that the model does not describe events without a hard scatter; these tend to be the lowest  $E_t$

events. At low energies, such as those studied here, the events not described by the simulation make up almost all of the cross section.

The first type of observable to be considered are the cross sections  $d\sigma/dE_t$  for different calorimeters. Each of the experiments studied has a large calorimeter which subtends some large angle along the beam axis, and completely surrounds the beam. The experiments can trigger on the  $E_t$  deposited into either the whole calorimeter, or some section extending only part way around the beam. We shall sometimes refer to these sections by the azimuthal angle they subtend. The smaller calorimeters tend to be most sensitive to jets in them. The  $2\pi$  calorimeters are sensitive both to events with jets of transverse momentum,  $p_t$ , slightly less than  $E_t/2$  and to nonjetlike events. These latter are both events of lower  $k_t$ , that is, transverse momentum generated at the hard scatter, where either more than the usual amount of bremsstrahlung has taken place, or some low  $p_t$  clusters have fragmented with high multiplicity. For example, at  $\sqrt{s} = 63$  about 3/4 of the cross section at  $E_t$  of 20 is from events with  $k_t < 6$ , with the remaining 1/4 coming from events with  $k_t$  up to about 9 GeV.

At these energies the cross section  $d\sigma/dk_t^2$  is a very steeply falling function of  $k_t$ . In addition to the  $1/k_t^4$  from the hard cross section there is, at these energies, a factor of  $(1-x_t)^{\alpha(Q^2)}$ , which comes from the wavefunction; it is the probability that there is a parton of enough energy to undergo the hard scatter.  $x_t$  is  $2k_t/E_{cm}$  and  $\alpha(Q^2)$  is at least 6 at  $Q_0^2$  and increases with  $Q^2$ . The result is that the cross section  $d\sigma/dk_t^2$  is a rapidly falling function of  $k_t^2$ . The parton events at any fixed  $k_t$  cover a range of values for any observable, for instance,  $E_t$  into some calorimeter. At any  $E_t$  in, say, a  $2\pi$  calorimeter the cross section comes both from events with  $k_t \approx E_t/2$ , most of which have transverse energy about  $E_t$ , and from the tail of events with lower  $k_t$  which fragment with

particularly high transverse energy. Because the cross section is so steeply decreasing, the small fraction of events at these lower  $k_t$ 's that hadronize to a system with transverse energy  $E_t$  have a strong influence. Those events tend to be ones with high amounts of bremsstrahlung or where either the beam jets or scattered jets are at the high end of the range for transverse momentum. That is, those events do not tend to look like four narrow jets. This is why, at low energy (NA5), high  $E_t$  events are not jetlike. At higher energies (for example, SPS)  $x_t$  is smaller and the  $(1-x)^a$  is not so important; the jets appear much more cleanly.

The experimental data and the results of the simulation are shown in Figs. 5.1-9. The agreement is reasonable or good in all cases except the  $2\pi$  calorimeter results from E-557, and, to a lesser extent, the  $4\pi/5$  calorimeter of that experiment. This experiment and AFS are in disagreement since E-557 report larger cross sections for fixed  $E_t$  than do the AFS collaboration, who have a larger calorimeter at the somewhat higher energy of 30 GeV. The  $2\pi$  calorimeter cross section at 30 GeV is about a factor of 2 lower than the experimental curve, corresponding to a shift in  $E_t$  of about a GeV.

That the simulation agrees with the experimental measurement of the cross section for both  $2\pi$  and smaller calorimeters over a range of energies is a strong indication that both jetlike and nonjetlike events appear with the correct cross section in the simulation.

At  $\sqrt{s}=63$  runs were made with two different gluon distributions, one that went as  $(1-x)^{10}$  as  $x \rightarrow 1$  and one that went as  $(1-x)^5$ . The simulation suggests that the  $(1-x)^5$  is preferred. The difference seems to come from the greater density of soft gluons for the  $(1-x)^{10}$ ; the larger cross section at high  $E_t$  come from events where a hard quark scatters off a soft gluon. The shape variables

were similar between the two runs.

Several different observables related to the shape of the events were studied at  $\sqrt{s} = 24, 30, \text{ and } 63 \text{ GeV}$ . As mentioned above, the accuracy of the simulation of the cross section for calorimeters subtending different azimuthal angles indicates that jetlike events occur at the correct rates, compared to the nonjetlike events.

Fig. 5.10 is a comparison of the mean charge multiplicity between the Monte Carlo and NA5 data. The agreement is moderately good, although the simulated values rise more slowly than do the measured values. The current simulation does better than previous work along these lines<sup>7</sup>, and than the predictions of a more naive model, where the event is just 4 Field Feynman jets<sup>4</sup>.

Fig. 5.11 shows the mean value of  $E_t$  into two back-to-back  $\pi/2$  sections of the NA5 calorimeter as a function of  $E_t$  into the other  $\pi/2$  sections. Both the simulation and the data reach a constant level, the simulation being slightly lower. The result of this simulation is significantly better than previous results. The experimental curve approaches the plateau from below, the simulation from above. This is an artifact of the simulation's requiring a parton scatter of  $k_t$  at least 2 GeV. Data with low  $E_t$  in a back-to-back region are, experimentally, dominated by low  $E_t$  events, which are not simulated by the Monte Carlo. In the Monte Carlo these events are dominantly those where the hard scattered partons are in the opposite direction.

Planarity is a measure of how much an event, projected onto the plane normal to the beam axis, resembles back-to-back jets. It is constructed from the transverse momentum tensor:

$$\begin{pmatrix} \sum p_x^2 & \sum p_x p_y \\ \sum p_x p_y & \sum p_y^2 \end{pmatrix}. \quad (5.1)$$

The sum is taken over all particles. The planarity is defined as:

$$P \equiv \frac{A-B}{A+B}, \quad (5.2)$$

where  $A$  and  $B$  are the larger and smaller eigenvalues of the transverse momentum tensor (this is a two dimensional analogue of sphericity.) A value of 1 indicates back-to-back jets, 0 a completely circular event. Fig. 5.12 shows the planarity distribution for events with  $E_t > 10$ , and Fig. 5.13, the mean planarity as a function of  $E_t$ . Both results are in good agreement with experiment.

Fig. 5.14 shows the mean total multiplicity in the AFS calorimeter compared with experimental measurements of  $E_t$  divided by the mean  $p_t$  measured in their drift chamber. The low  $E_t$  events agree well with experiment; the high  $E_t$  events seem to have a lower multiplicity than the experimental measurement. What this indicates about the shortcomings of this simulation is discussed below.

Fig 15 shows the mean circularity ( $1 - \text{planarity}$ ) as a function of  $E_t$ . The simulated events become too jetlike at too low an  $E_t$ . Again, the significance of this is discussed below.

Figs. 16-17 show the circularity distributions at  $\sqrt{s} = 63$  for two bins of  $E_t$ , starting at 6 GeV, in one wall of the calorimeter. In the lower bin, 6 to 8.5 GeV of transverse energy in the calorimeter, the events are somewhat too planar. In the other bin they are far too planar. The problems with the shapes variables at high  $E_t$  are discussed in the next section.

All these discrepancies are consistent with the high  $p_t$  jets fragmenting into too few particles with too much  $p_t$  per particle. This would make the jets narrower, hence the events less circular. The mean multiplicity would also be reduced at high  $E_t$ . It would have little effect on  $d\sigma/dE_t$  in the different

calorimeters, as even the small ones are much larger than a jet. The mean  $p_t$  per particle was measured at the AFS in regions (in azimuth) toward, away from, and normal to the thrust axis. The Monte Carlo calculations of the same quantities showed that the mean  $p_t$  per particle in both the forward and away directions was 20% to 30% higher than the measured value. This gives further indication that the problem with the shape variables is that the high  $p_t$  jets fragment with too low a multiplicity.

Preliminary studies indicate that the trouble is caused by the treatment of the gluons, in particular, the fact that even soft gluons split color strings. When a string, say the string connecting a final quark to the rest of the event, is broken by a soft gluon, the mass of the resulting cluster is not much larger than the mass of the final quark, that is below  $\sqrt{t_{cut}}$ . A cluster this light can produce only a few particles on hadronization. On the other hand, had the soft gluon not been radiated (or had it not split the string), the cluster would have had a much larger mass and hadronized into more particles.

There is much evidence to suggest that the disagreement with experiment is, indeed, caused by the treatment of the gluons. The shape variables in the region where the disagreement with experiment is most pronounced are sensitive to changes in the conditions and cutoffs governing the splitting of gluons, like the cutoff scale for radiation  $t_{cut}$ . For example, if one refuses to split gluons of less than some fixed energy, the agreement with experiment is much improved. Likewise, if one puts all the final state gluons at zero mass, so that soft gluons which are split get recombined because the clusters left behind are below the cutoff, the agreement is much improved. Earlier work using parton showers with a different model, with several *ad hoc* assumptions to reduce the number of light clusters caused by splitting from soft gluons, for fragmenting

gluons was able to reproduce the experimental result more closely<sup>7</sup>.

The treatment of gluons used here is intuitively unappealing in some respects. Splitting gluons into quark antiquark pairs is completely artificial, and allows soft gluons to break the string connecting, for example, a quark and an antiquark. In the studies of  $e^+e^-$  and NA5 it seems adequate to choose the cutoffs such that there is not much soft radiation. The results of this study indicate that in areas sensitive to hard gluons this method of reducing the influence of the soft gluons is inadequate. The events with hard gluons are more sensitive to the treatment of the soft gluons, since the hard gluons radiate far more gluons than either soft gluons or quarks, whether hard or soft.

There is neither a calculation, nor an intuitive QCD based explanation for the splitting of gluons, and certainly no basis to prefer one algorithm for doing so to another on the basis of any theoretical grounds. One would strongly prefer a model which is not very sensitive to such technical assumptions. In such a model the soft gluons would become unimportant naturally and there would be no need to adjust the technical assumptions to make them unimportant. We are beginning to investigate other treatments of the gluons, that is, other ways to model the division of parton final states with gluons into low mass color singlet clusters which will then decay by phase space models. These methods will be discussed in chapter 6. The shape variables in high energy  $pp$  scattering seem to be a good place to test new models.

The other area in need of improvement is the beam remnant. In the simulation the mean  $p_t$  per particle in the normal region was about 75 MeV (out of 400) lower than the experimental result. This result, as well as the low plateau for the  $\langle E_{t_{out}} \rangle$  at 24 GeV, suggests that the beam remnants are somewhat too narrow. While the model of the beam jet used here seems reasonable, though not

good, at these energies, it predicts a multiplicity distribution at  $\sqrt{s} = 540$  which is far narrower than the UA1 measurements.

It is difficult to find theoretical guides for modeling the beam remnant. It may well be that the best one can do is parametrize the experimental data. If this is so more data on the structure of the high multiplicity events at UA1 will be needed to parametrize the beam jets at collider energies. Possible improvements to the treatment of the beam remnant are discussed in chapter 6.

## References for chapter 5

- [1] F. W. Büsser, et al., *Phys. Lett.* **46B** (1973), 471. See also Ref. 4.
- [2] R. P. Feynman, Field, R. D. and Fox, G. C., *Phys. Rev.* **D18** (1978) 3320.
- [3] C. Bromberg, et al., *Phys Rev Lett.* **38** (1977) 1447; *Nucl. Phys.* **B134** (1978) 189; *Phys. Rev. Lett.* **43** (1979) 565; *Nucl. Phys.* **B171** (1980) 1.
- [4] C. De Marzo, et al., *Nucl. Phys.* **B211** (1983) 375.
- [5] B. Brown, et al., Fermilab preprint FERMILAB-Conf-82/34-EXP, presented by C. Halliwell at XVII Rencontre de Moriond. (1982).
- [6] T. Akesson, et al., CERN Preprint CERN-EP/83-71 (1983); Rafe H. Schindler, *Proc. of the 10<sup>th</sup> SLAC Summer Institute on Particle Physics*, A. Mosher, ed. (1983) 371.
- [7] R. D. Field and G. C. Fox, Invited talk presented at the Europhysics Study Conference on Jet Dynamics in Quark and Lepton Interactions, Erice, Sicily, Sep. 1982, and references therein.

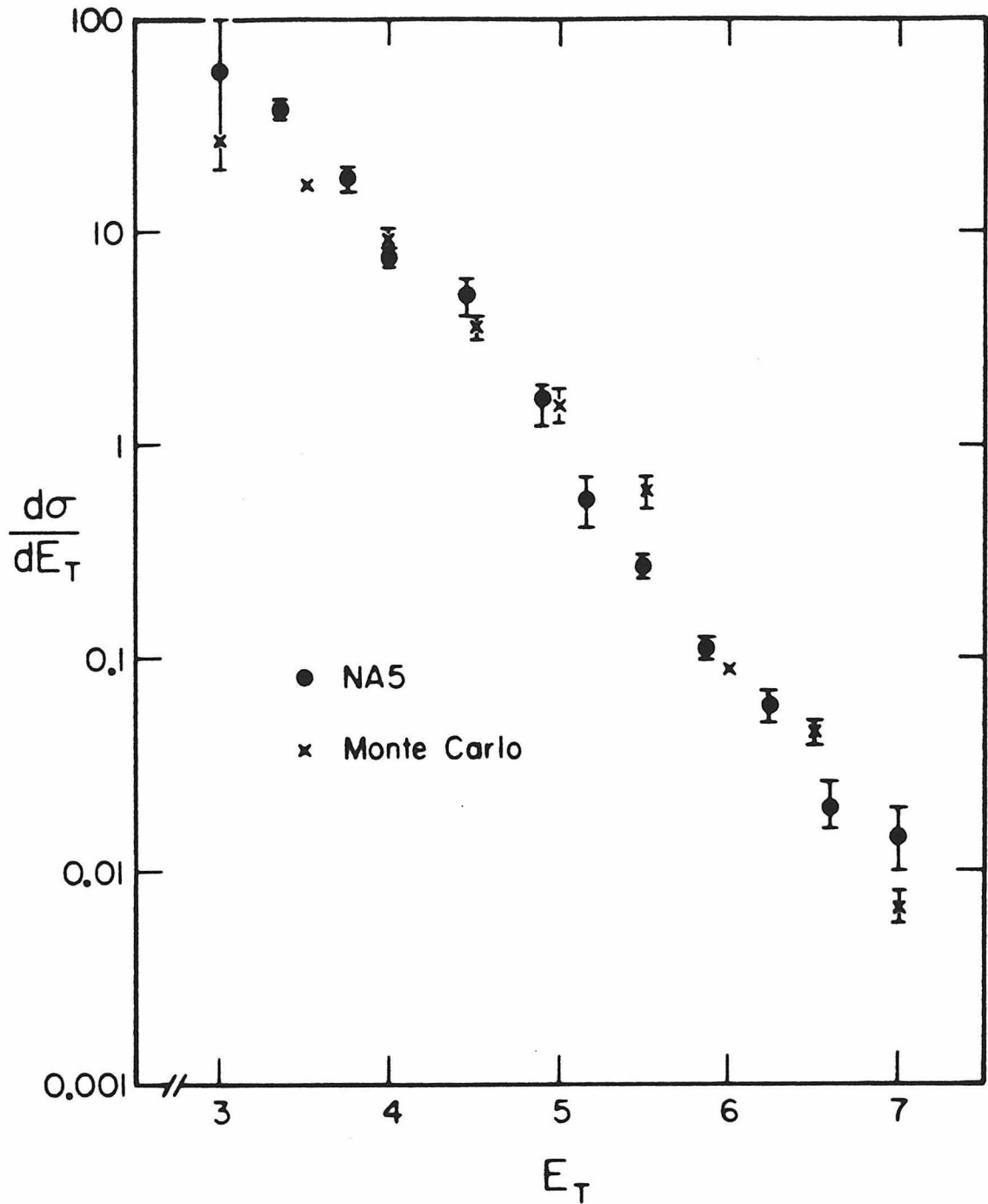


Fig. 5.1:  $d\sigma/dE_T$ , in microbarns/GeV, in a  $\pi/2$  section of the NA5 calorimeter compared with the simulation,  $\sqrt{s} = 23.76$  GeV.

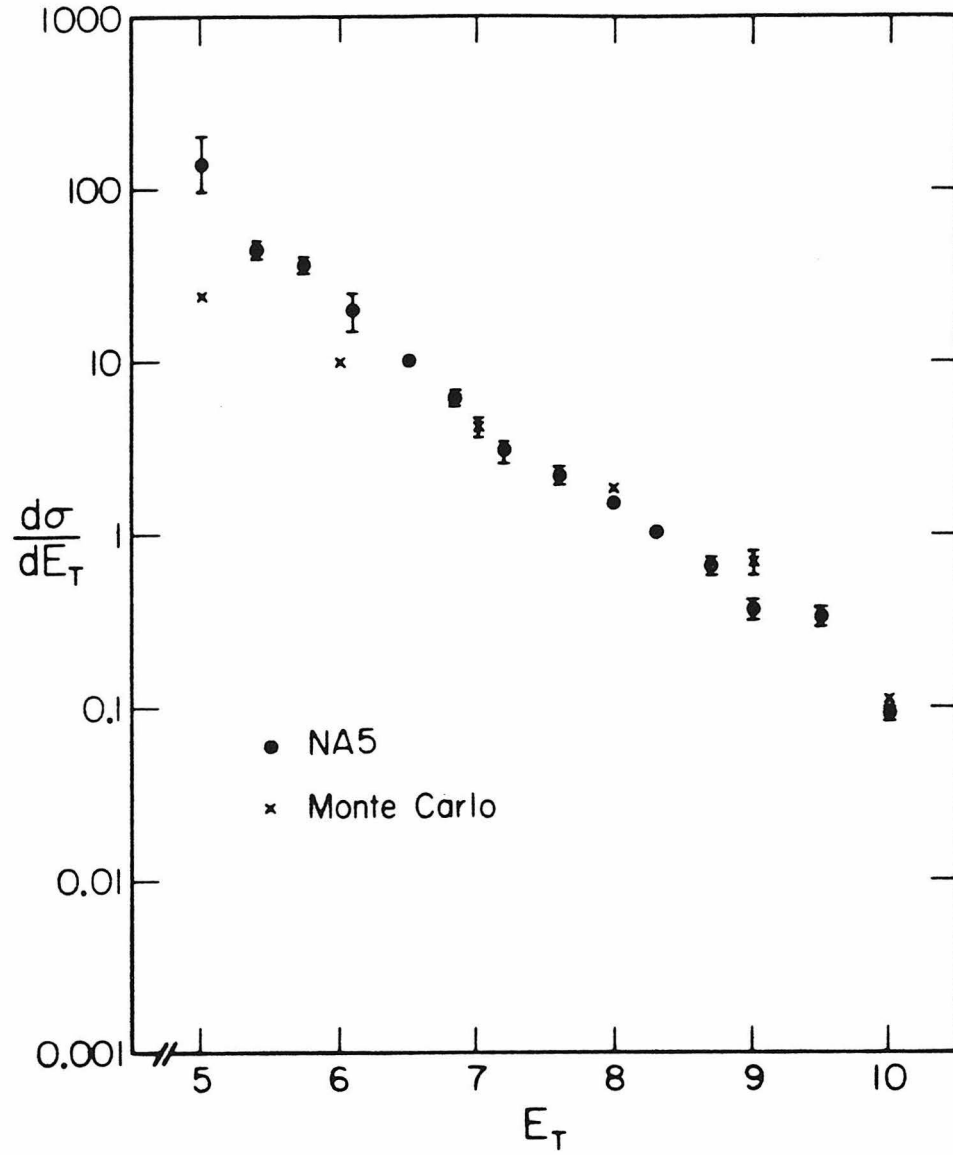


Fig. 5.2:  $\frac{d\sigma}{dE_T}$ , in microbarns/GeV, in back-to-back  $\pi/2$  sections of the NA5 calorimeter compared with the simulation,  $\sqrt{s} = 23.76$  GeV.

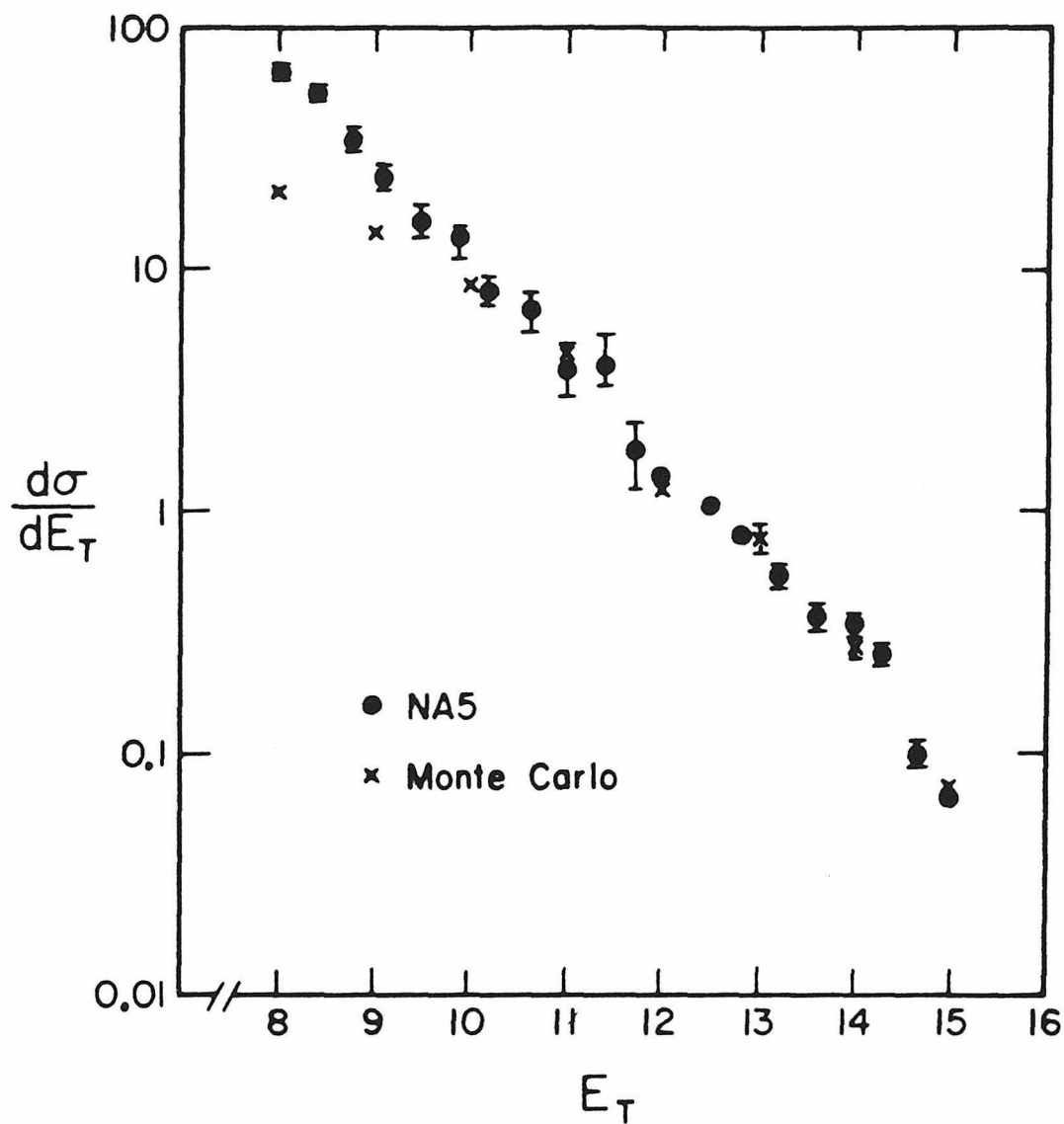


Fig. 5.3:  $\frac{d\sigma}{dE_T}$ , in microbarns/GeV, in the NA5  $2\pi$  calorimeter compared with the simulation,  $\sqrt{s} = 23.76$  GeV.

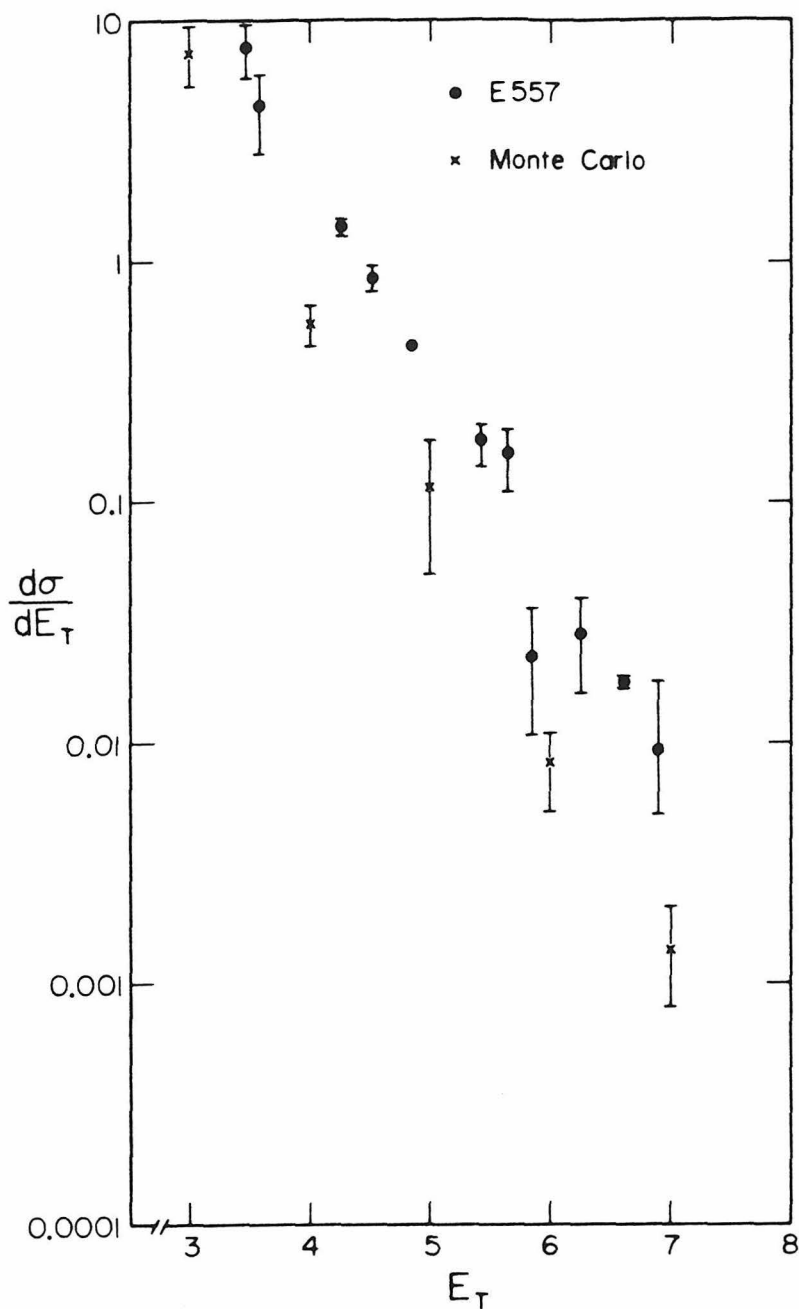


Fig. 5.4:  $\frac{d\sigma}{dE_T}$ , in microbarns/GeV, in the  $\pi/5$  calorimeter of E-557, compared with the simulation,  $\sqrt{s} = 27.43$  GeV.

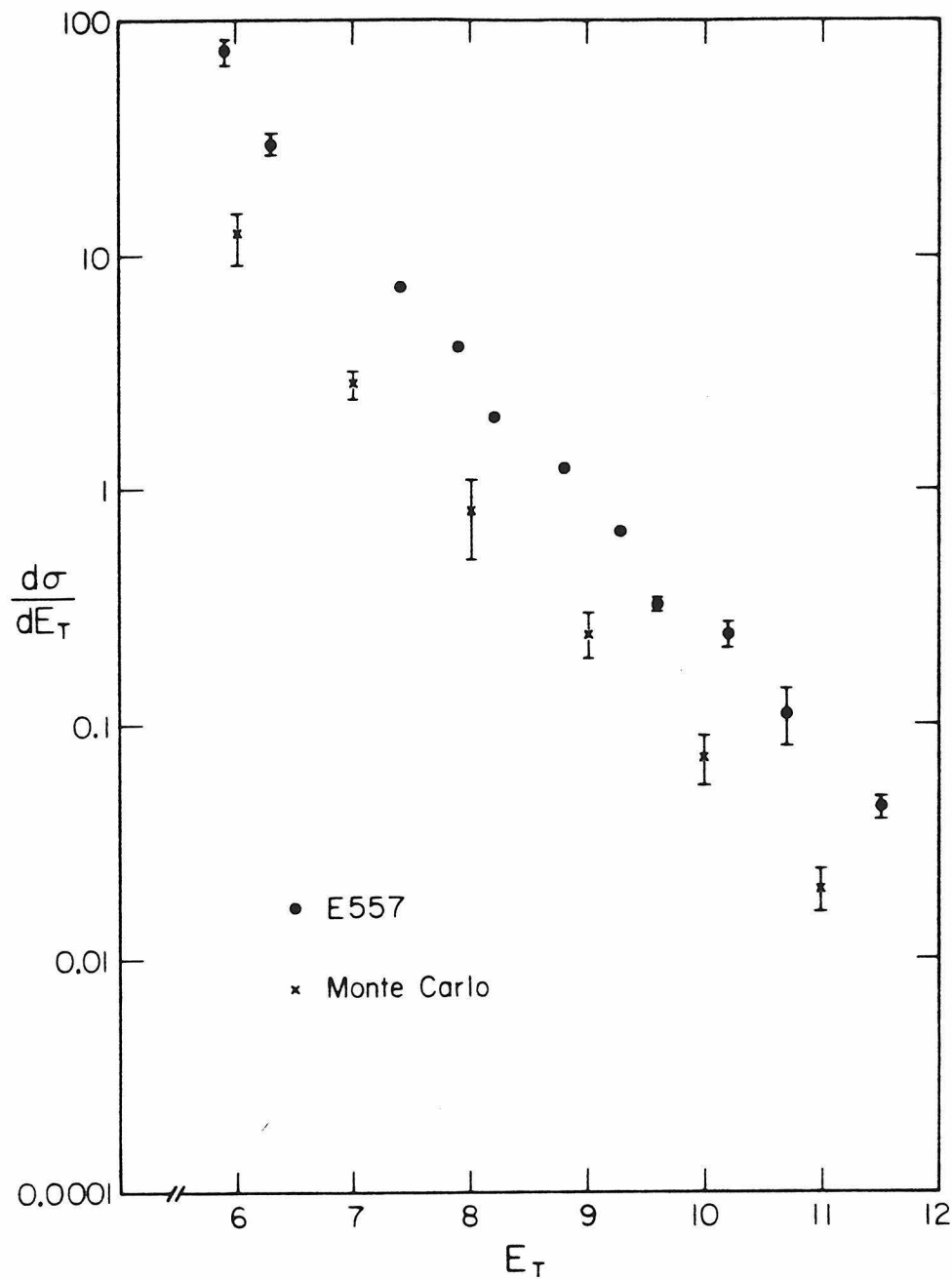


Fig. 5.5:  $\frac{d\sigma}{dE_T}$ , in microbarns/GeV, in the  $4\pi/5$  calorimeter of E-557, compared with the simulation,  $\sqrt{s} = 27.43$  GeV.

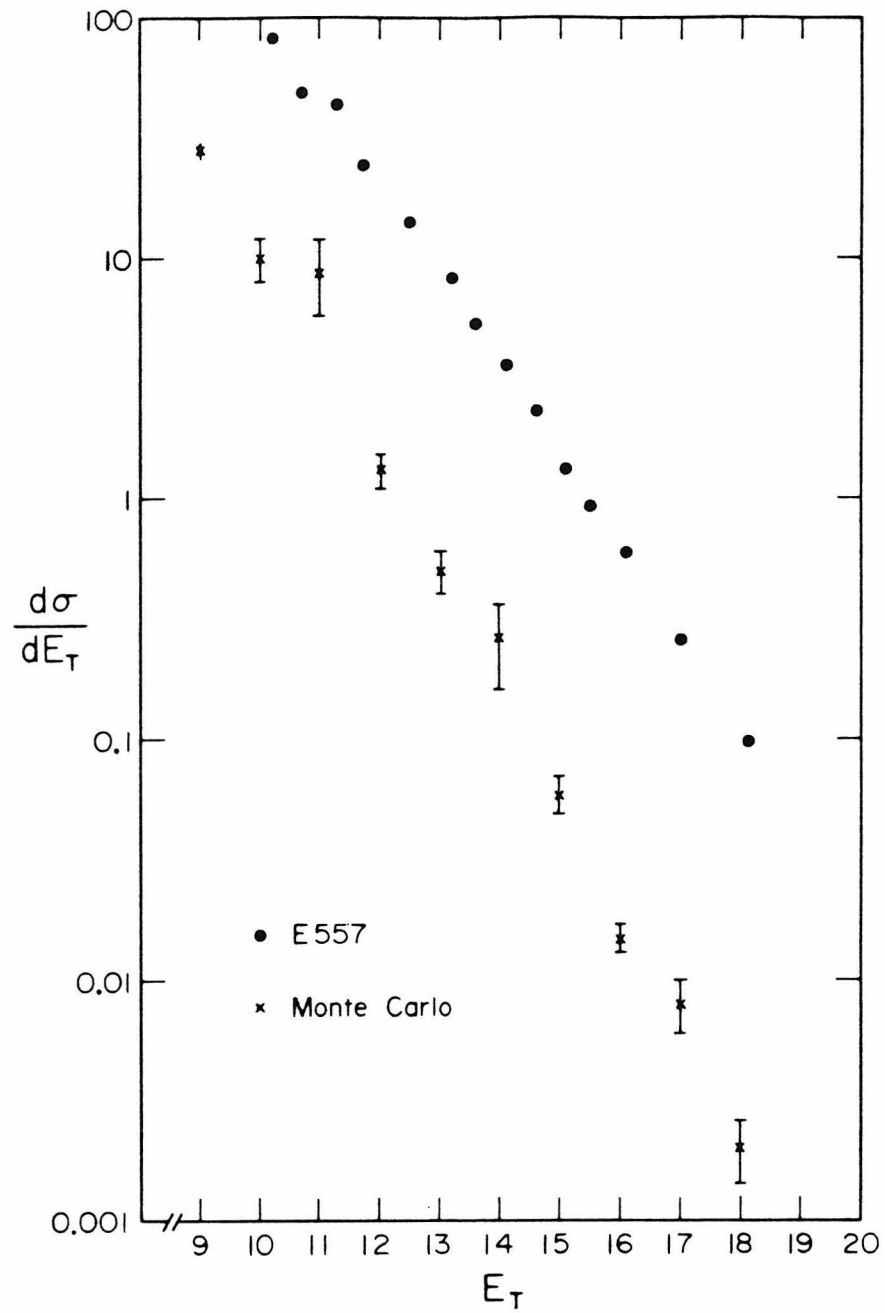


Fig. 5.6:  $d\sigma/dE_T$ , in microbarns/GeV, in the  $2\pi$  calorimeter of E-557, compared with the simulation,  $\sqrt{s} = 27.43$  GeV.

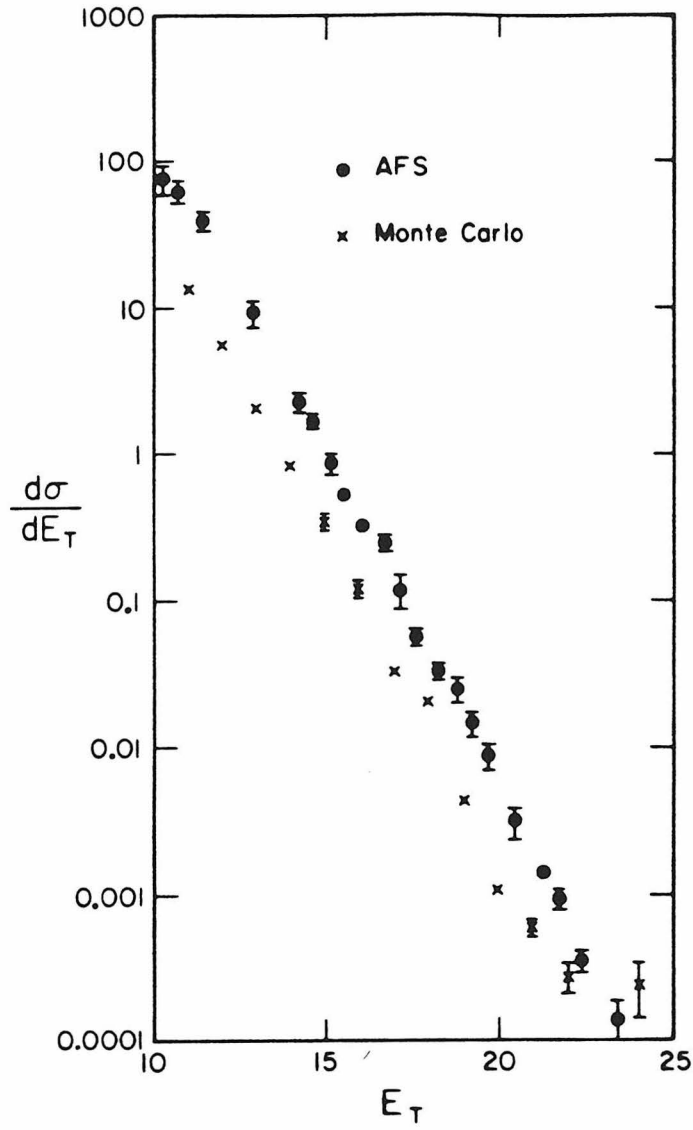


Fig. 5.7:  $d\sigma/dE_T$ , in microbarns/GeV, in the  $2\pi$  calorimeter of the AFS group, compared with the simulation,  $\sqrt{s} = 30$ . GeV.

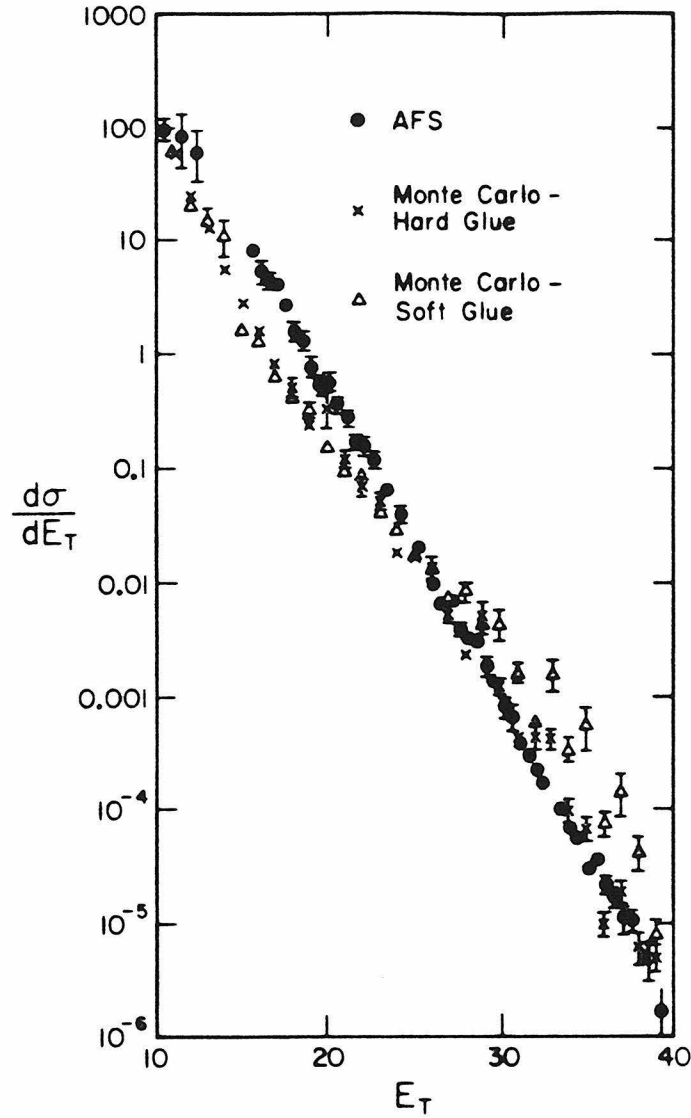


Fig. 5.8:  $d\sigma/dE_T$ , in microbarns/GeV, in the  $2\pi$  calorimeter of the AFS group, compared with the simulation,  $\sqrt{s} = 63$ . GeV. The points labeled hard glue are with the  $(1-x)^5$  distribution function for gluons, those labeled soft glue with the  $(1-x)^{10}$  distribution.

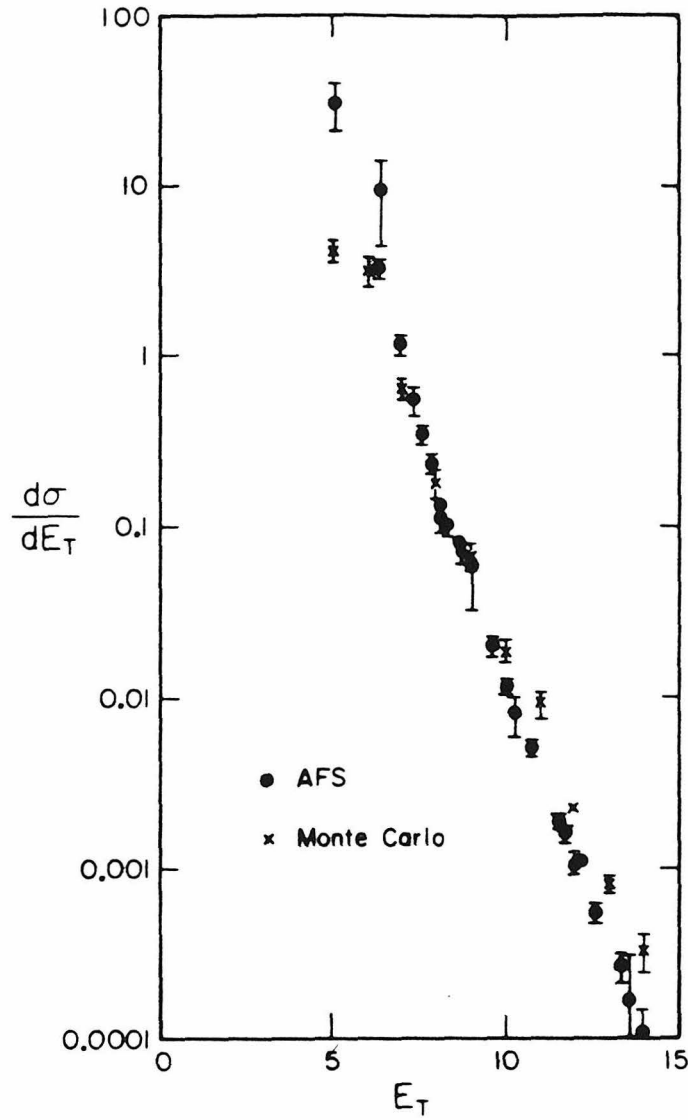


Fig. 5.9:  $d\sigma/dE_T$ , in microbarns/GeV, in one wall of the calorimeter of the AFS group, which subtends an azimuthal angle of  $69^\circ$ , compared with the simulation,  $\sqrt{s} = 63$ . GeV.

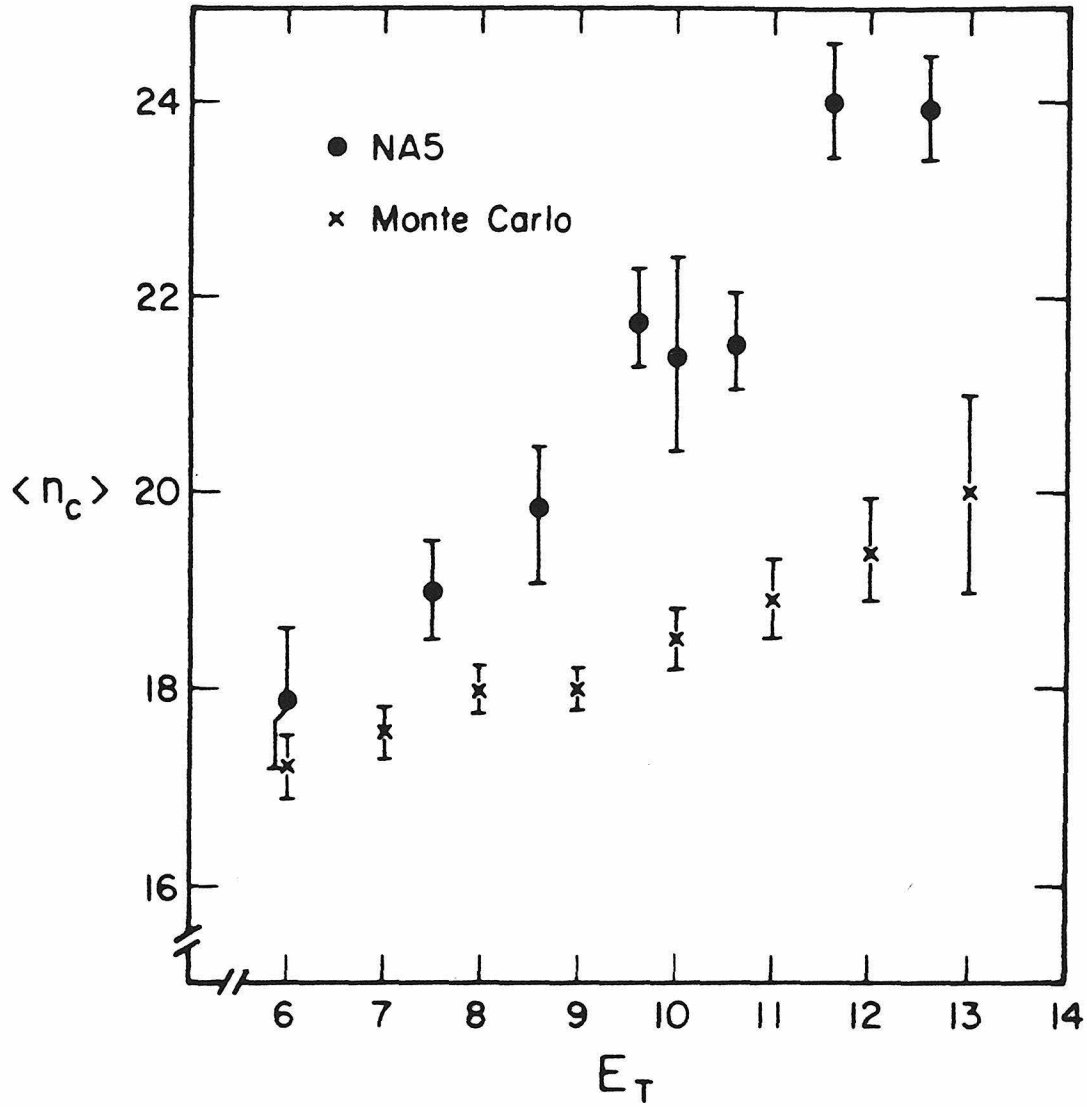


Fig. 5.10: Mean charged multiplicity vs.  $E_T$ , in GeV, in the NA5  $2\pi$  calorimeter, compared with the simulation.

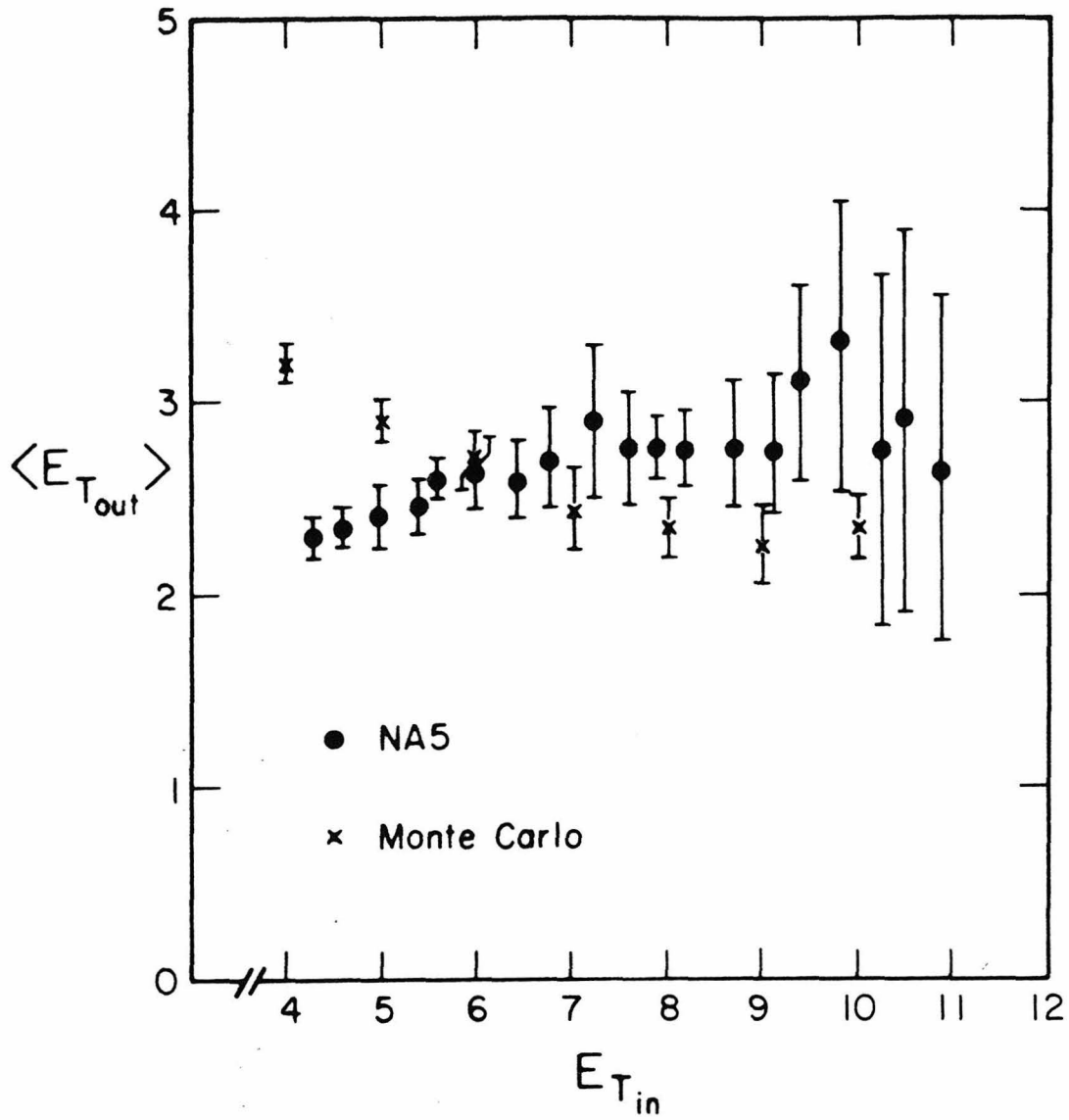


Fig. 5.11: Mean  $E_t$ , in GeV, out of back-to-back  $\pi/2$  sections of the NA5 calorimeter, that is, in the other  $\pi/2$  sections, vs.  $E_t$ , in GeV, in the 2 sections, compared with the simulation.

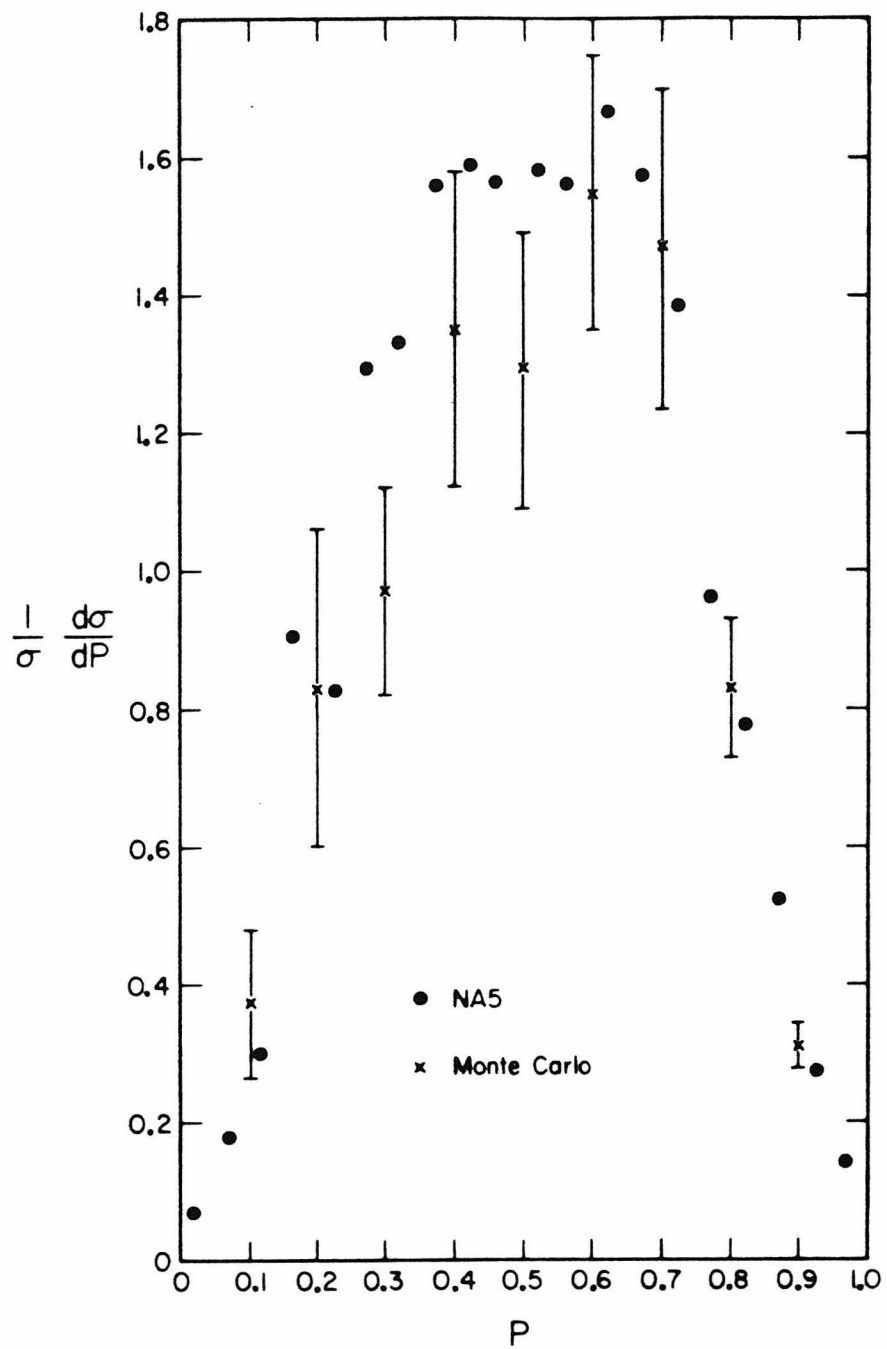


Fig. 5.12: Planarity distributions for events with  $E_t > 10$  GeV, in the NA5  $2\pi$  calorimeter, compared with the simulation.

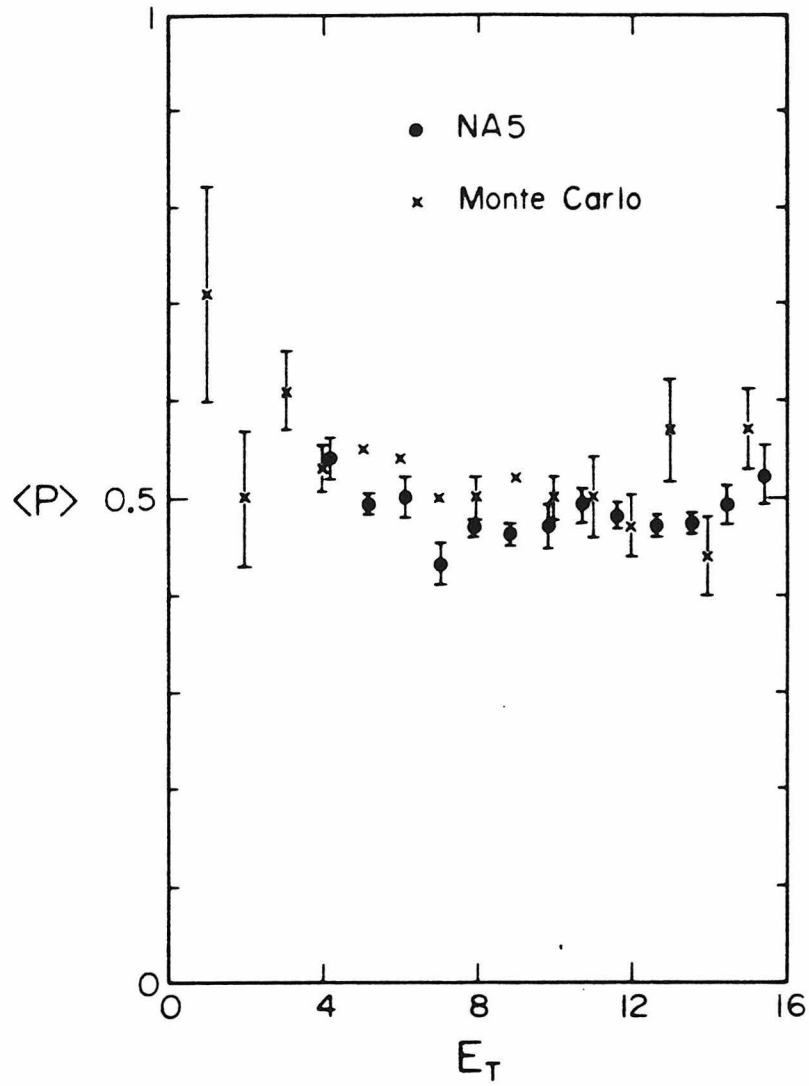


Fig. 5.13: Mean planarity vs.  $E_T$ , in GeV, in the NA5  $2\pi$  calorimeter, compared with the simulation.

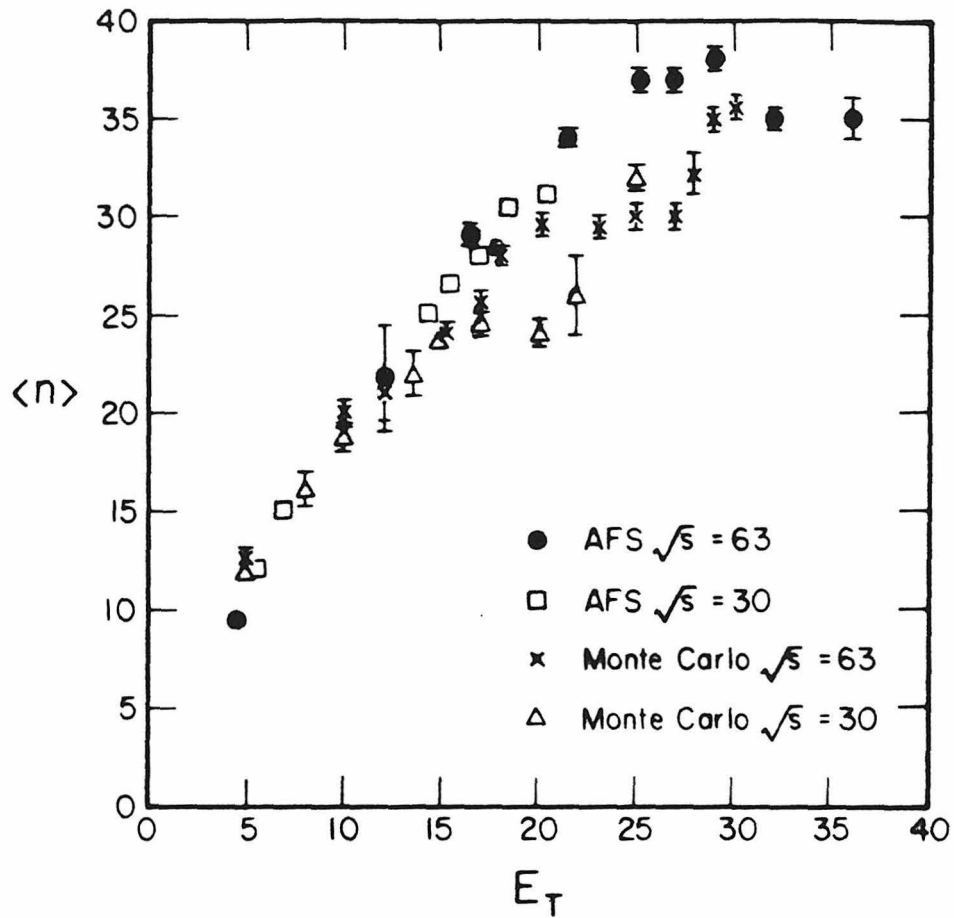


Fig. 5.14: Simulated values of total multiplicity in the full AFS calorimeter, compared with experimental measurements of  $E_T$  divided by mean  $p_t$  per track in the drift chamber.

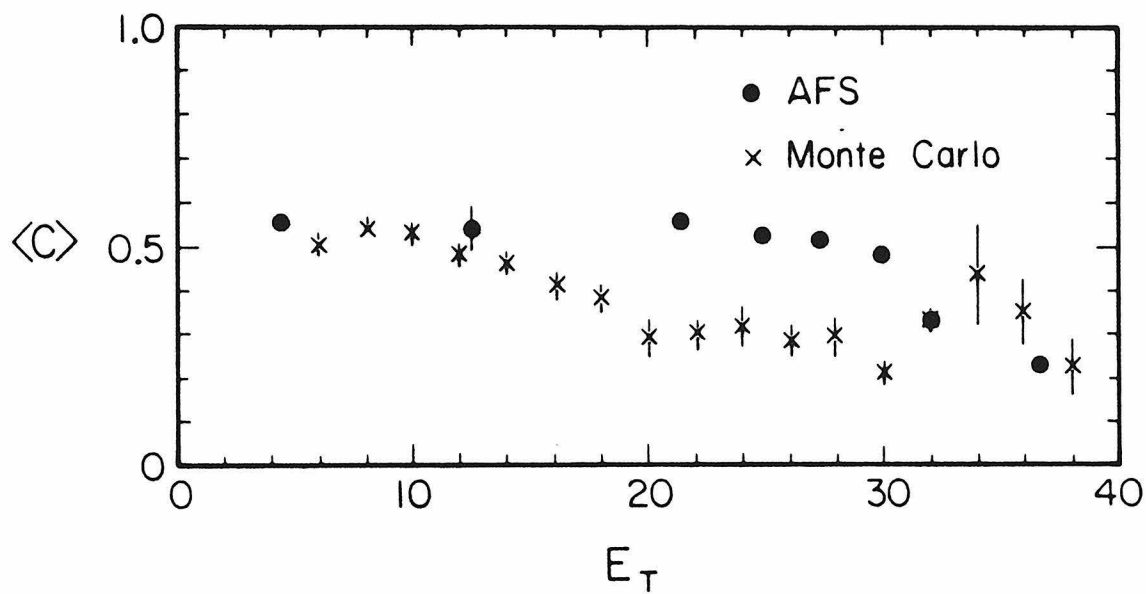


Fig. 5.15: Mean circularity vs.  $E_T$ , in GeV, in the full AFS calorimeter, compared with the simulation.  $\sqrt{s} = 63$

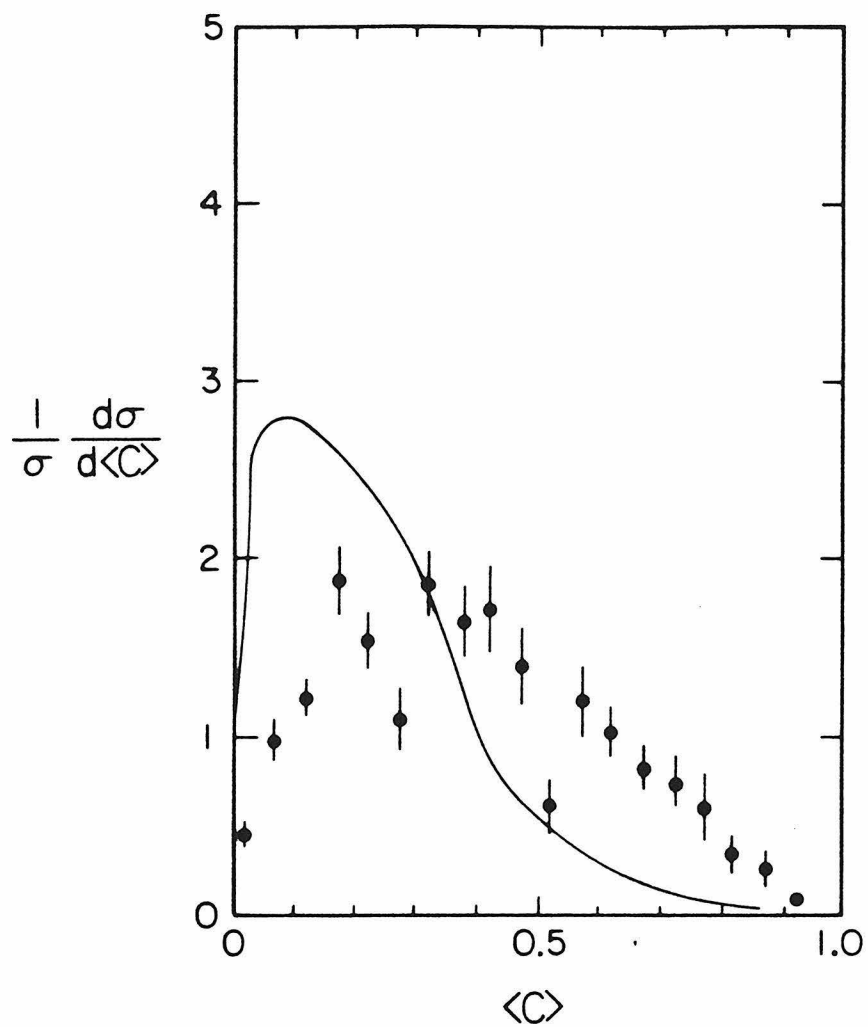


Fig. 5.18: Circularity distribution for events which deposit  $E_t$  between 6.0 GeV and 8.5 GeV in one wall of the AFS calorimeter, compared with the simulation.  $\sqrt{s} = 63$  GeV. The curve is the simulated results, the points are measured data.

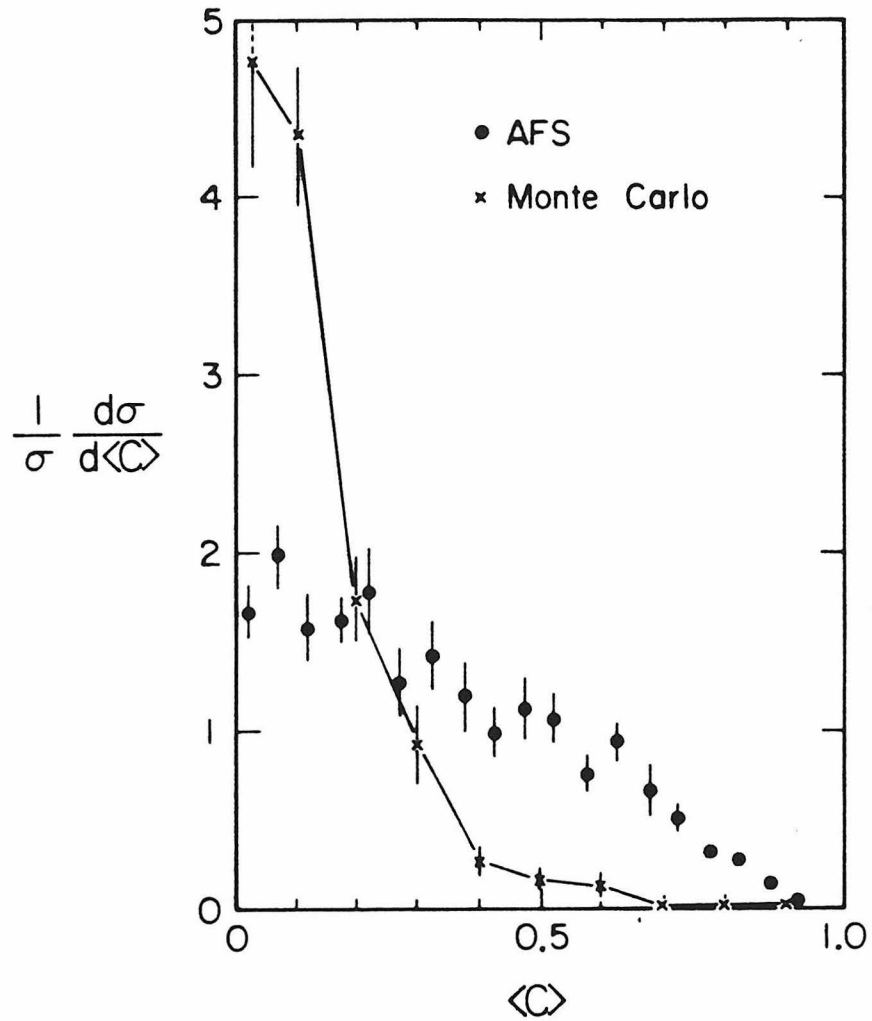


Fig. 5.17: Circularity distribution for events which deposit  $E_t$  between 8.5 GeV and 11 GeV in one wall of the AFS calorimeter, compared with the simulation.  $\sqrt{s} = 63$  GeV. The line is drawn through the Monte Carlo points to guide the eye.

## **6. Discussion and conclusions**

### **6.1. Areas of phenomenological concern**

The study reported in chapter 5 shows that the model described above is moderately successful in describing high  $E_T$  hadron hadron scattering at ISR energies and below. There are some difficulties at these energies caused by the treatment of the gluons, as discussed above. If one tries to extend the model to collider energies, there is trouble with the beam remnants.

#### **6.1.1. Treatment of gluons**

The first issue is to correct the hadronization of the gluons. As we noted in chapter 5, allowing soft gluons to split the color strings connecting the partons has severe phenomenological problems. It produces clusters of too small a mass, giving too few particles. In addition, it makes the predictions of the model very sensitive to the number of soft gluons produced, for which the predictions of the perturbation expansion are not reliable.

As an extreme example of the effects of soft gluons, consider a string connecting a quark and an antiquark; let each parton have a mass of 300 MeV and the system have an invariant mass of 30 GeV, a typical PETRA energy. If no gluon is radiated the system will evolve by string breaking to a few clusters, giving rise to an event with about 20 hadrons. If an arbitrarily soft gluon, say with an energy of 1 eV, is radiated, we would have two clusters, each with a mass of 300 MeV. These could only give rise to a state with 4 pions.

Allowing a perturbatively generated soft gluon to have such a strong effect is not only phenomenologically wrong, but it is inconsistent with the spirit of the model. Perturbative QCD can only describe hard physics accurately; in the

model the behavior of soft gluon fields is meant to be described by the string model or parametrized by the phase space model. It is not described by perturbation theory. A better model than the one we used would be one in which the gluons naturally become unimportant as they become soft, so that perturbatively generated soft gluons have no effect.

One such model is to treat the gluons as kinks in the string, as is done in the Lund picture described above. If one did not allow the strings to break, the motion of the partons, acted on by the string tension, would describe a complicated 2-dimensional surface in spacetime, the world surfaces of the strings. One could then imagine allowing the string to break with uniform probability per unit area, allowing only for cuts to insure that any remnant has enough mass for its flavor. There would be a strong tendency for the string to break in the region of a hard gluon where it is significantly stretched. Near a soft gluon the string is not stretched so much; as the gluon gets softer its influence becomes less.

### **6.1.2. The beam remnant**

The beam remnant is governed by low transverse momentum physics; it is not described well by perturbative QCD. One can hope to describe it by phenomenological models based on QCD ideas. As was mentioned above, the model tried here, while moderately successful up to ISR energies, was not successful at collider energies. There are several difficulties with the model at collider energy (540 GeV). In the first place, the multiplicity distribution is not as expected. If one plots probability for an event with  $n$  particles (or  $n$  charged particles) *vs.*  $n / \langle n \rangle$ , for low energy data, the plot is roughly independent of the center of mass energy<sup>1</sup>. This is called KNO scaling<sup>2</sup>. At the collider the KNO plot is much broader than at lower energy<sup>3</sup>. Also there is a rise in the

average multiplicity as the transverse momentum per particle increases that is more than can be explained by events with hard bremsstrahlung<sup>4</sup>. There is, as yet, no phenomenological model that can explain both the high energy and the low energy data, so the best one can do is to fit the data at each energy.

The approach used also has some severe theoretical problems. In a hadron hadron event there are the two beam remnants, and the two scattered partons, and whatever partons arise from radiation from these or from the partons with spacelike momentum before the hard scatter, all separating from one another. Initially all these are colored; then the color screens. In principle, all these interact. In the model described above, the two beams exchange some momentum, and their color is screened against a fairly soft gluon radiated by the active partons heading toward the hard scatter. There is no reason, if the exchange of momentum is really present that it should not involve the scattered jets as well. In fact, in spacetime, the beam remnant, and most of the strings formed by partons radiated as the active parton from that hadron evolves to the hard scatter, are, at the time when the interactions get strong, on top of one another, given the finite widths of the strings. One thus ought to expect the hadronization of these strings to influence one another. In that case one needs some model for the hadronization of such a system.

One idea that begins to address these issues, once the soft gluons do not break the strings, is to treat the beam remnant as part of a baryonic string that is connected to the remainder of the event as dictated by the evolution. In this model the beam remnant is connected to the radiated quanta. When the string breaks, probably near some hard radiation, the beam remnant would be left in a substring with the softer radiation in a very massive substring, which would then hadronize. This model may not go far enough. The model will only group the

beam remnant and the attendant radiation as a substring part of the time, as determined by the string breaking model. Other times the beam remnant may be separated from the radiation by the first string break. It might be necessary to force the beam remnant and attendant radiation to hadronize together, separate from the partons coming from the hard scatter or hard radiation.

## 6.2. Other concerns

### 6.2.1. Better perturbative approximations

We should use better approximations to perturbative QCD than those that were used. It is known that the leading log approximation is accurate only very close to the collinear limit<sup>5</sup>, and that higher order corrections are important<sup>6</sup>. In  $e^+e^-$  it is possible to use the full perturbative cross section to order  $\alpha_s^2$ , or higher, if it were computed, at least at PETRA energies. This is possible since states with more than 4 partons are not very important; there are no 5 jet events. In hadron hadron scattering, and  $e^+e^-$  at higher energy, where many parton events are important, it is not practical to compute perturbation to high enough order. It is important to incorporate subleading terms into the vertices of the decay chain to make them as accurate as possible. Some steps in this direction were taken in this model by the particular choice made for  $z$ , the  $E+|p|$  fraction, which does reproduce the most important subleading term in  $e^+e^- \rightarrow q\bar{q}G$ . More work needs to be done in this area.

All that would be required to use a more accurate approximation for the hard scattering cross section would be to compute the higher order perturbative corrections to the  $2 \rightarrow 2$  matrix elements by the usual procedures.

Since, in hadron hadron scattering, hard radiation is most likely to occur near the hard scatter (that's where the partons are furthest off shell) it might be a good idea to treat the hard scatter as a  $2 \rightarrow n$  process to whatever order perturbation theory has been calculated; the leading log approximation would describe the evolution of the partons going into, and the partons emitted from the hard scatter. Care would have to be taken to avoid double counting.

### 6.2.2. Cutoffs and a spacetime picture

We have already remarked that the resolvability cutoffs used are theoretically questionable. The use of mass cutoffs to determine whether a cluster decays by the string breaking picture or the phase space model and where a string can break is also arbitrary. There is some evidence from heavy flavor production in  $e^+e^-$  annihilation that a mass cutoff is not correct<sup>7</sup>. It has been suggested that spacetime constraints might be better<sup>7</sup>. If so, it might be advantageous to use a spacetime picture to determine all the cutoffs, as well as to determine which partons overlap in the hadronization process and should, therefore, be considered together.

A spacetime model would have some theoretical advantages besides providing a better picture of the cutoffs. The soft hadrons are produced before the parton evolution has finished. The hard partons have moved away from the region where the soft hadrons are formed, but the slowest among them can still be close enough to the region where the soft hadrons form, within the intrinsic size of the strings, for the partons and forming hadrons to affect one another. A spacetime model of hadronization would allow us to address this issue. Developing such a model might improve our understanding of the hadronization process.

### 6.3. Conclusions

We have found hadron hadron scattering to be a useful place to study aspects of QCD models not tested in the cleaner arena of  $e^+e^-$ . The ability of the cluster model, which was developed for  $e^+e^-$ , to reproduce many features of the data without adjusting parameters, is an indication that the model is based on sound ideas. We have found, however, several aspects of the model which are unsound. We have shown where the model must be improved to increase its reliability.

### References for Chapter 6

- [1] K. Goulianos, H. Sticker and S. N. White, *Phys. Rev. Lett.* 42 (1982) 1454.
- [2] Z. Koba, H. B. Nielsen, and P. Olesen, *Nucl. Phys.* B40(1972)
- [3] K. Bockmann, Talk given at the 3<sup>rd</sup> International Conference on Physics in Collisions, Como, Italy, 1983.
- [4] G. Arnison, *et al.*, *Phys. Lett.* 118B (1982) 167.
- [5] T. D. Gottschalk, E. Monsay and D. Sivers, *Phys. Rev.* D21 (1980) 1799.
- [6] W. Bartel, *et al.*, *Phys. Lett.* 119B (1982) 239.
- [7] T. D. Gottschalk, *Nucl. Phys.* B238 (1984) 349.

## Appendix—Use of the Monte Carlo Program

This appendix describes the particular Monte Carlo Program described in the text and used in the investigations reported in chapter 5. A tape of the program is available from G. C. Fox. The tape is in the *tar* format for UNIX machines.

The program is organized into several basic modules. The first step is to input the data and organize the calculation. The values of  $k_t^2$  are stepped through; for each value the following modules are called:

- 1: A collection of partons is evolved to the scale  $Q^2=4k_t^2$ . During this stage a large disk file is created to store the information about the partons associated with the SLP and a smaller one, containing a summary of the set of final SLPs generated, is also created. The program can be set to remove these as it goes along.
- 2: The collection of final SLPs is gone through to find a set of hard scatters. When a suitable set is found they are evolved, one by one, to the cutoff. A disk file containing these events is written.
- 3: Each event, calculated at the parton level, is then run through a routine which puts in the beam remnants and forms the initial clusters.
- 4: The clusters are hadronized according to a QCD cluster model. The output of the hadronizer is contained in the common block *prtcls*. The weight of each event is in the common block *sigma*. The final events are written to disk.

The disk files of final partons and final events are for calculating observables. The observables could be calculated on an event by event basis within the main loop, avoiding the need for writing these large files if it were so desired.

The files are found in several directories on the tape; FORTRAN and, sometimes, ratfor source is provided. There is one C program. The main directory contains the main loop (in *qcdmain*), the routine to input data, *setup*, a routine *tree* which takes the output of the parton shower, forms the initial clusters and calls routines *beamj* and *flavs* to setup the beam remnants and then calls the hadronizer. There are also some utility programs to calculate Lorentz and vector algebra and a program *dump.c* to do rapid I/O with the disk. The parton shower code is found in the directory *parton*. The hadron code is found in the directory *hadron*. The directory *cb* contains common blocks for the routines. In addition to the routines supplied, a function *ranf()* that returns a random number between one and zero is needed. The seed for the random number generator is set by *ranseed(integer)*, and *iseed()* should return a seed.

The routines which a user is likely to wish to modify are the ones in the main directory, and *xint* in the *parton* directory which gives  $\int_{\xi}^1 f(x)dx$ , the integral of the user supplied distribution functions, and the routines it calls.

The subroutine *tree* takes the information from the parton shower (in common block *cjet*) and finds clusters and effective quarks and antiquarks in them which are stored in common blocks *sngltz* and *klstrs*; the soft hadrons produced by the beam jet routines are in common block *prtcls*. There are comment cards in the common blocks which should explain the variables. The code for hadron types is supplied with the tape.

The version supplied on this tape is that described in the text; i. e., the beam jets and the gluons have the problems alluded to in the text. When a version of the hadronizer with the proposed treatment of the gluons is available, it will be included on the tape.

The input required by the program is as follows:

**read (5, \*) iwhat,nf,ntries,jprt,nprfl**

**iwhat** should be set to 15. **nf** is the number of flavors that can be produced. **ntries** is the number of partons with spacelike momentum with energy above the cutoff to be generated before trying to combine them. **jprt** is a print argument passed on to *tree*; 0 is recommended. **nprfl** is how many full events (at the parton level) are printed.

**read (5, \*) qsq,tcut,alam2,(xmasq(i),i=1,nf)**

**qsq** is not used. **tcut** is the mass cutoff for resolvable radiation from time-like partons. **alam2** is  $\Lambda^2$ . The **xmasq(i)** are the masses of the quarks.

**read (5, \*) jseed**

**jseed** is the seed given to *ranset*. A value less than 1 means get the seed from *iseed*.

**read (5, \*) ecm,q0sq,ec1,ec2**

Respectively, the center of mass energy, the scale  $Q_0^2$  at which the partons are extracted, no longer used, and the energy cutoff for radiation from partons with spacelike momentum

**read (5, \*) nprgd,nprbd,nball,iec1tp,kttype,iprtp**

**nprgd** is how many good jets (up to hard scatter) are printed. **nprbd** is how many bad jets (up to hard scatter) are printed. (Bad means that the parton radiates to an energy below the cutoff.) **nball** is how many bad jets (up to hard scatter) are allowed, a value of -1 means as many as needed, which is what should be used. **iec1tp** and **kttype** should be set to 0. **iprtp** should be 0 for a  $p\bar{p}$  scattering and 1 for  $pp$  scattering.

**read (5,\*) finprt, evprnt**

These logical variables control some debugging prints in the main program.

They should be set false

**read(5,\*) (disfun(j,i),j=1,10) for 6 cards**

These are the distribution functions for valence  $u$ , valence  $d$ , light sea quarks,  $s$  and  $\bar{s}$  quarks, charmed quarks, and gluons, one per line. The first nine entries on each line determine the  $x$  distribution; they are three sets each of the form  $a_1 x^{a_2} (1-x)^{a_3}$  which are added together. The tenth entry is  $\pi \langle k_t \rangle^2$ . The (real) values for  $a_3$  are rounded to the nearest integer for convenience.

**read(5,"(a32)") file(i) for 6 lines**

These are file names. Each is a prefix to which a character is added which depends on which  $k_t$  region the file refers to. The first is for the collections of particles associated with the partons with spacelike momentum; the second, for the summary of parton with spacelike momentum properties. The fourth is for the final events at the parton level; the fifth, for the hadron level. The other 2 are no longer used.

**read (5,\*) maxev**

The number of hard scatters in each region of  $k_t$ . The actual number of events generated may be slightly less than this because of roundoff errors.

**read (5,\*) bfud(1),bfud(2),beamwd,fudflg**

Some parameters for the beam jet, respectively: the amount of momentum transferred between the jets when the active parton is a quark, and a gluon. The amount of transverse momentum for the soft hadrons relative to the remnants. This should be very small ( $\lesssim 0.01 \text{ GeV}^2$ ), and a flag which should

be false.

**read (5,\*) ktlow,kthi,nokt**

The first two are real variables, the upper and lower values for the  $k_t^2$  integration. The third is the number of regions to divide the range into.

There is one more integer read in by the main loop after all these parameters. It is the number of regions for which to delete the information about the partons with spacelike momentum after it is no longer needed.